GigaScience

Multi-dimensional leaf phenotypes reflect root system genotype in grafted grapevine over the growing season

--Manuscript Draft--

Manuscript Number:	GIGA-D-21-00137R3
Full Title:	Multi-dimensional leaf phenotypes reflect root system genotype in grafted grapevine over the growing season
Article Type:	Research
Funding Information:	National Science Foundation (1546869) — Dr Allison J. Miller

Abstract:

Background: Modern biological approaches generate volumes of multi-dimensional data, offering unprecedented opportunities to address biological questions previously beyond reach due to small or subtle effects. A fundamental question in plant biology is the extent to which below-ground activity in the root system influences above-ground phenotypes expressed in the shoot system. Grafting, an ancient horticultural practice that fuses the root system of one individual (the rootstock) with the shoot system of a second, genetically distinct individual (the scion), is a powerful experimental system to understand below-ground effects on above-ground phenotypes. Previous studies on grafted grapevines have detected rootstock influence on scion phenotypes including physiology and berry chemistry. However, the extent of the rootstock's influence on leaves, the photosynthetic engines of the vine, and how those effects change over the course of a growing season, are still largely unknown.

Results: Here, we investigate associations between rootstock genotype and shoot system phenotypes using five multi-dimensional leaf phenotyping modalities measured in a common grafted scion: ionomics, metabolomics, transcriptomics, morphometrics, and physiology. Rootstock influence is ubiquitous but subtle across modalities with the strongest signature of rootstock observed in the leaf ionome. Moreover, we find that the extent of rootstock influence on scion phenotypes and patterns of phenomic covariation are highly dynamic across the season.

Conclusions: These findings substantially expand previously identified patterns to demonstrate that rootstock influence on scion phenotypes is complex and dynamic and underscore that broad understanding necessitates volumes of multi-dimensional data previously unmet.

Corresponding Author:	Zachary N Harris Saint Louis University SAINT LOUIS, MO UNITED STATES
Corresponding Author Secondary Information:	
Corresponding Author's Institution:	Saint Louis University
Corresponding Author's Secondary Institution:	
First Author:	Zachary N Harris
First Author Secondary Information:	
Order of Authors:	Zachary N Harris
	Mani Awale
	Niyati Bhakta
	Daniel H. Chitwood
	Anne Fennell
	Emma Frawley
	Laura L. Klein

	Laszlo G. Kovacs
	Misha Kwasniewski
	Jason P. Londo
	Qin Ma
	Zoë Migicovsky
	Joel F. Swift
	Allison J. Miller

Order of Authors Secondary Information:	

Response to Reviewers:	1.We have added information into the Code Availability Section so that it now meets the required format. 2.All figshare links were added to the references. Additionally, the GigaDB citation was added to the references. These are all referenced in the Availability of Data section. We also lightly edited the Availability of Data Section to be less redundant. 3.Abbreviations, Competing Interests, and Funding information has all been added/moved to the appropriate sections.

Additional Information:	
Question	**Response**
Are you submitting this manuscript to a special series or article collection?	No
Experimental design and statistics Full details of the experimental design and statistical methods used should be given in the Methods section, as detailed in our Minimum Standards Reporting Checklist. Information essential to interpreting the data presented should be made available in the figure legends. Have you included all the information requested in your manuscript?	Yes
Resources A description of all resources used, including antibodies, cell lines, animals and software tools, with enough information to allow them to be uniquely identified, should be included in the Methods section. Authors are strongly encouraged to cite Research Resource Identifiers (RRIDs) for antibodies, model organisms and tools, where possible. Have you included the information	Yes

requested as detailed in our [Minimum Standards Reporting Checklist](#)?	
Availability of data and materials All datasets and code on which the conclusions of the paper rely must be either included in your submission or deposited in [publicly available repositories](#) (where available and ethically appropriate), referencing such data using a unique identifier in the references and in the "Availability of Data and Materials" section of your manuscript. Have you have met the above requirement as detailed in our [Minimum Standards Reporting Checklist](#)?	Yes

1 **Multi-dimensional leaf phenotypes reflect root system genotype in grafted**

2 **grapevine over the growing season**

3

4 Zachary N. Harris[1,2*] (zachary.n.harris@slu.edu), Mani Awale[3] (maybd@mail.missouri.edu), Niyati

5 Bhakta[1,2] (niyatisbhakta@gmail.com), Daniel H. Chitwood[4,5] (chitwoo9@msu.edu), Anne Fennell[6]

6 (anne.fennell@sdstate.edu), Emma Frawley[1,2] (emma.frawley@wustl.edu), Laura L. Klein[1,2]

7 (laura@leafworks.com), Laszlo G. Kovacs[7] (laszlokovacs@missouristate.edu), Misha Kwasniewski[3]

8 (mtk5407@psu.edu), Jason P. Londo[8] (jason.londo@usda.gov), Qin Ma[9] (qin.ma@osumc.edu), Zoë

9 Migicovsky[10] (zoe.migicovsky@dal.ca), Joel F. Swift[1,2] (joel.swift@slu.edu), and Allison J. Miller[1,2*]

10 (allison.j.miller@slu.edu)

11

12 [1]Department of Biology, Saint Louis University, 3507 Laclede Avenue, St. Louis, MO, 63103-2010, USA

13 [2]Donald Danforth Plant Science Center, 975 North Warson Road, St. Louis, MO, 63132-2918, USA

14 [3]Division of Plant Sciences, University of Missouri, 135 Eckles Hall, Columbia, MO, 65211, USA

15 [4]Department of Horticulture, Michigan State University, East Lansing, MI, 48824, USA

16 [5]Department of Computational Mathematics, Science and Engineering, Michigan State University, East

17 Lansing, MI, 48824, USA

18 [6]Department of Agronomy, Horticulture & Plant Science, South Dakota State University, Brookings, SD,

19 57006, USA

20 [7]Department of Biology, Missouri State University, 901S. National Avenue, Springfield, MO, 65897,

21 USA

22 [8]United States Department of Agriculture, Agricultural Research Service: Grape Genetics Research Unit,

23 630 West North Street, Geneva, NY, 14456-1371, USA

24 [9]Department of Biomedical Informatics, The Ohio State University, 1585 Neil Ave, Columbus, OH,

25 43210

26 [10]Department of Plant, Food, and Environmental Sciences, Faculty of Agriculture, Dalhousie University,

27 Truro, NS, B2N 5E3, Canada

28 * To whom correspondence should be addressed

29
30
31
32
33
34
35

Abstract

Background: Modern biological approaches generate volumes of multi-dimensional data, offering

unprecedented opportunities to address biological questions previously beyond reach due to small or

subtle effects. A fundamental question in plant biology is the extent to which below-ground activity in the

root system influences above-ground phenotypes expressed in the shoot system. Grafting, an ancient

horticultural practice that fuses the root system of one individual (the rootstock) with the shoot system of

a second, genetically distinct individual (the scion), is a powerful experimental system to understand

below-ground effects on above-ground phenotypes. Previous studies on grafted grapevines have detected

rootstock influence on scion phenotypes including physiology and berry chemistry. However, the extent

of the rootstock's influence on leaves, the photosynthetic engines of the vine, and how those effects

change over the course of a growing season, are still largely unknown.

Results: Here, we investigate associations between rootstock genotype and shoot system phenotypes

using five multi-dimensional leaf phenotyping modalities measured in a common grafted scion: ionomics,

metabolomics, transcriptomics, morphometrics, and physiology. Rootstock influence is ubiquitous but

subtle across modalities with the strongest signature of rootstock observed in the leaf ionome. Moreover,

we find that the extent of rootstock influence on scion phenotypes and patterns of phenomic covariation

are highly dynamic across the season.

Conclusions: These findings substantially expand previously identified patterns to demonstrate that

rootstock influence on scion phenotypes is complex and dynamic and underscore that broad

understanding necessitates volumes of multi-dimensional data previously unmet.

Background

        High-throughput data acquisition has afforded unprecedented capacity to quantify and understand

plant form and function. Recent advances in imaging and computation have expanded our ability to

measure plant traits or phenotypes [1,2], and to extend those comprehensive measurements into latent

2

62   space phenotypes [3]. Now broadly known as phenomics, this burgeoning field is characterized as the

63   acquisition and analysis of high-dimensional phenotypic data at different hierarchical levels [4,5], often

64   with an eye toward multiscale data integration. A holistic and hierarchical approach to plant phenotypic

65   variation affords unique insights into plant evolution and how plants change over development and in

66   response to environmental cues and horticultural manipulation.

67   A fundamental question in plant biology is how root systems influence phenomic variation in

68   above-ground shoot systems including leaves, flowers, and fruits. Grafting, a common horticultural

69   manipulation that joins the shoot system of one individual (the scion) with the root system of another

70   individual (the rootstock), is commonly used in crop species to confer favorable phenotypes to

71   commercial scions [6], including enhanced disease resistance [7,8], fruit quality, plant form [9], response

72   to water stress [10], and growth on particular soils [11,12]. Because grafting often uses clonally

73   propagated materials, it is possible to manipulate and replicate different combinations of root systems and

74   shoot systems, offering a valuable experimental system in which root system impacts on shoot system

75   phenotypes can be evaluated.

76   The European grapevine (*Vitis vinifera*) is among the most economically important grafted crops

77   in the world. Grapevines are cultivated primarily for fruits used to make wine and juice, as well as for

78   table grape and raisin production. Grafting in grapevines became widespread in the mid-1800's following

79   the accidental introduction of the root-feeding aphid phylloxera from its native North America into

80   Europe, where it began attacking the roots of European grapevines [13]. Because European grapevines

81   often do not survive phylloxera infestation, in regions where phylloxera has been introduced most

82   grapevine cultivation consists of European grapevines grafted to rootstocks derived from phylloxera-

83   resistant North American *Vitis* species including *V. berlandieri, V. riparia,* and *V, rupestris*, and their

84   hybrid derivatives. In addition to grapevines, more than 70 major perennial crops are grafted including

85   many fruit trees and vines [9]. Grafting decouples the breeding of shoot systems and root systems, with

86   selection in plants targeted for use as scions focusing primarily on fruit phenotypes, and selection in

87 plants targeted for use as rootstocks focused on below-ground biotic and abiotic stress resistance, as well

88 as their impacts on shoot system phenotypes.

89 The effects of grafting in grapevine show a remarkable breadth of scion response patterns. For

90 example, a study of *Vitis vinifera* cv. 'Cabernet Sauvignon' grafted to different rootstocks identified

91 transcriptome reprogramming in the scion of grafted plants; this appeared to be a general effect of

92 grafting to a rootstock and was not rootstock-specific [14]. In contrast, other studies have found

93 signatures of rootstock genotype in the transcriptome in early berry development, although this distinction

94 was lost in later development [15,16], but see [17]. Comprehensive phenomic analyses, including those

95 that link transcriptome data with other high-throughput phenotyping assays, offer an opportunity to

96 expand understanding of rootstock effects on grapevine shoots. In one study, leaves of the *V. vinifera*

97 cultivar 'Gaglioppo' showed variation in stilbene and abscisic acid concentrations due to rootstock

98 genotype, as well as differences in transcriptional profiles [18]. Likewise, gene expression, ion

99 concentrations, and leaf shape in the cultivar 'Chambourcin' varied in response to rootstock genotype

100 [18,19]. Collectively, these studies suggest the impacts of grafting are diverse and may vary over the

101 course of vine development. However, to date few studies have surveyed multiple high-dimensional scion

102 phenotypes to understand rootstock influence on shoot system phenotypes over the course of the growing

103 season or the extent to which grafting effects on the scion covary with one another.

104 Leaves are the photosynthetic engine of the organism and a primary site for perception and

105 response to environmental change. Grapevine leaves have been used for centuries as markers of species

106 and cultivar delimitation, developmental variation, disease presence, and nutrient deficiency [20,21].

107 More recently, analysis of grapevine leaf morphology has identified genetic architecture of leaf shapes

108 [22], developmental patterns across the season [23], and signatures of evolution in the grapevine genus

109 [24]. Grapevine leaves respond to stress through gas and water exchange with the atmosphere [25,26] and

110 have been shown to differentially partition the ionome depending on their position on the shoot [19] and

111 their rootstock genotype [19,27,28]. The volume of work on grapevine leaves provides a foundation for

112 the analysis of phenomic variation in a vineyard over a season in response to grafting.

113   In this study, we investigate effects of grafting on high dimensional leaf phenotypes of the hybrid

114   cultivar 'Chambourcin' over the course of the growing season. We quantify leaf elemental (ion)

115   concentrations, metabolite abundance, gene expression, shape, and vine physiology in a replicated

116   rootstock trial where the hybrid grapevine cultivar 'Chambourcin' is growing ungrafted and grafted to

117   three different rootstocks. The four root-shoot combinations ('Chambourcin' ungrafted, 'Chambourcin'

118   grafted to three different rootstocks) are replicated 72 times in a randomized block experimental design

119   with an irrigation treatment (Supplemental Figure 1). Phenotypic data, data that describe variation for a

120   particular trait within a particular modality, were collected either on the full 288-vine set (ion

121   concentrations, leaf shape) or on a subset of 72 vines (the 72-vine set; metabolite abundance, gene

122   expression, vine physiology). Using data collected at three time points that span the growing season

123   (anthesis, veraison, and harvest), we show that all phenotyping modalities (ionomic, metabolomic,

124   transcriptomic, morphometric, and physiology phenotypes) reflect subtle but ubiquitous responses to

125   grafting and rootstock genotype. Rootstock effects on shoot system phenotypes were often dynamic

126   across the season, suggesting that accounting for seasonal variation could enhance our understanding of

127   grafting effects in viticulture.

128

129   **Data Description**

130

131   *Leaf Ionomics*

132   The ionome describes elemental composition of a tissue at a particular time point [29]. Three

133   leaves per vine were collected from the 288-vine set at three seasonal time points: anthesis (~mid May),

134   veraison (~late July), and harvest ~mid September). Leaves were sampled from a single shoot and

135   included the youngest fully opened leaf at the shoot tip, the approximate middle leaf, and the oldest leaf at

136   the shoot base. Teams were deployed in the vineyard so that multiple vineyard rows were being sampled

137   concurrently. As such, 'block' represented unmeasured spatial variation, but did not strictly correlate with

138   time of sampling due to the nature of sampling (see Methods). Whole leaves were placed in zip-lock bags

139   in the field and stored in a cooler on ice packs, scanned for leaf shape analysis in the lab (see Leaf Shape)

140   and then dried in coin envelopes at 50°C for one to three days for elemental analysis. Between 20 and 100

141   mg of leaf tissue was acid digested and 20 ions were quantified using inductively coupled plasma mass

142   spectrometry (ICP-MS) following standard protocol of the Donald Danforth Plant Science Center

143   (DDPSC) Ionomics Pipeline [30,31]. Ion quantifications were corrected for internal standard

144   concentrations, instrument drift and by initial sample mass. The output of the Pipeline contained

145   estimated concentrations of each of the following 20 elements: Al, As, B, Ca, Cd, Co, Cu, Fe, K, Mg, Mn,

146   Mo, Na, Ni, P, Rb, S, Se, Sr, and Zn. For each ion concentration, we computed z-score distributions and

147   used those values as the basis for linear models. Following convention, non-standardized values were

148   used for machine learning analysis.

149

150   *Leaf Metabolomics*

151   The metabolome comprises small mostly organic molecules present in a tissue and represents a

152   catalogue of the products of metabolic processes [32,33]. Metabolomic analysis was completed at

153   veraison (the onset of fruit ripening) and immediately prior to harvest for the 72-vine set. For each vine,

154   three mature leaves were sampled from the middle of a single shoot and immediately flash frozen in

155   liquid nitrogen in the field to capture the metabolic state of the leaves when attached to the vine. Leaves

156   were sampled by a single team near midday in row and block order, ensuring that 'block' captured both

157   unmeasured spatial variation and temporal variation over the sampling window (see Methods). Frozen

158   leaves were transported to the University of Missouri Enology Lab on dry ice and stored at -80˚C.

159   Following the protocol of [34], whole leaves were manually ground in liquid nitrogen with a mortar and

160   pestle, 0.5g of powder was weighed into a centrifuge tube, 1.5ml of 1:1 MeOH: ACN was added.

161   Samples were vortexed to suspend leaf particles and sonicated for 20 minutes in an ice bath. After

162   extraction, samples were centrifuged for 10 minutes at 3,000 g and filtered with a 0.22 PTFE syringe filter

163   into a 1.5ml sample vial before injecting into a Waters XEVOTM QToF LCMS system (Waters

164 Corporation, Milford, MA, USA). Chromatographic separation was achieved using a Waters Acquity TM

165 Ultra Performance LC H-Class system (Waters Corporation, Milford, MA, USA) equipped with Waters

166 Acquity BEH C18 column (2.1mmx150mm and 1.7um particle size) and a diode array detector. Samples

167 were injected in random order across the sampling periods. The injection volume was set at 2.5ul and the

168 flow rate was set at 0.4 ml/min. The mobile phase consisted of 0.1% formic acid in water (solvent A) and

169 0.1% formic acid and 5% water in acetaldehyde (solvent B) and the gradient was as follows: 100% A for

170 0.5 min; 0.5-18min increased to 99% B; 18-19 min. held at 99% B; mobile phase was re-equilibrated for

171 2 min between runs. Diode array was monitored at 225-500nm. Mass spectrometry was performed on a

172 XevoTM QTof (Waters Corporation, Milford, MA, USA). The electrospray ionization (ESI) was operated

173 in both positive or negative ionization modes in separate runs. The scan range was set as m/z 50-1500

174 with 0.2 sec accumulation time. MS settings were as follows: capillary voltage was 2.5kV; cone voltage

175 ramped from 20-40V; collision energy was set to 6V; detector voltage was set to 1950V; desolvation gas

176 was set to 1000 L/hour; cone gas was set to 50 L/hr; source temperature was 120℃ and desolvation

177 temperature was set at 550℃.

178   LC-MS instrument files were converted to .cdf format and uploaded to XCMS online [35] for

179 chromatogram normalization and feature detection via "single job" parameters. The 661 identified

180 metabolomic features were used as the basis of a principal components (PC) analysis. The top 20 PCs

181 were treated as distinct phenotypes to model according to the experimental design. In PCs that varied

182 significantly by rootstock, features that loaded more than 1.96 standard deviations above or below the

183 mean were fit independently with the same model design.

184 *Leaf Gene Expression*

185   The youngest fully-opened leaves on two shoots were collected from each plant of the 72-vine set

186 (see Study Design). The two leaves, which were distinct from leaves used for ionomics, leaf shape,

187 metabolomics and physiology data collection, were pooled for RNA sequencing. Leaves were sampled by

188 a single team near midday between 10AM and 2PM in row order, ensuring that 'block' and 'row'

189   accounted for unmeasured spatial variation and temporal variation over the sampling window (see

190   Methods). Samples were sequenced using 3'-RNAseq, a method ideal for organisms with reasonably

191   characterized reference genomes [36]. Total RNA was extracted from plant tissues using the Sigma

192   Spectrum Plant Total RNA kit with modification of the addition of 2% PVP40 to the extraction buffer to

193   decrease phenolic inhibitors. All RNA extractions were checked for quality control using a Nanodrop.

194   Sequencing was conducted using the Illumina NextSeq500 platform which returned single-end 86 bp

195   reads. To accommodate the large number of samples in this study, we opted to obtain fewer reads per

196   sample, which might have limited our ability to detect differential expression in lowly-expressed genes.

197   The first 12 nucleotides from each read were trimmed to remove low-quality sequences using

198   Trimmomatic (options: HEADCROP:12; [37]). Low quality trimmed reads were additionally identified

199   based on overrepresentation of kmers and removed using BBduk (April 2019 release) [38]. Trimmed and

200   QC-controlled reads were mapped to the 12Xv2 reference *Vitis vinifera* genome [39,40] using STAR

201   (v2.7.2b) [41] with default alignment parameters. RNAseq read alignments were quantified using HTSeq-

202   count (v0.11.2) [42] and a modified version of the VCost.v3 reference *V. vinifera* genome annotation

203   [40]. To capture mis-annotated gene body boundaries in the genome, all gene boundaries in the

204   annotation were extended 500 bp.

205   Variation in gene expression was assessed using two methodologies. First, we identified

206   individual genes which responded to specific factors in the experimental design using DESeq2 (v1.24.0)

207   [43]. Each gene was fit with the model "~ Block + Irrigation + Phenology_Rootstock" where the

208   'Phenology_Rootstock' model term was used to understand the potential interaction of phenology and

209   rootstock. Genes were filtered to a gene set that included only genes with a normalized count greater than

210   or equal to two in at least five samples. To check the validity of our expression results, we assayed two

211   classes of housekeeping genes (Ubiquitin-domain and actin-family) and eight previously annotated

212   circadian genes [44] (Supplemental Figure 2). Differentially expressed genes were identified for each

213   pairwise contrast in the model. Second, we used principal component analysis (PCA) to collapse variation

214   in co-expressed genes into fewer dimensions. Normalized count-filtered genes from DESeq2 were

215 transformed using the variance stabilizing transformation (VST; [45]) and input into a PCA. We then

216 analyzed the top 100 PCs in the context of the broader experimental design. We previously showed that

217 the transcriptome varied by the time of collection and was potentially interacting with the rootstock effect

218 [19]. Moreover, the other modalities in this study point to weak if any effects from the irrigation treatment

219 (see Supplemental Note 1). Due to the nature of the vineyard design, we could not identify both irrigation

220 and time effects (marked by row) in a single model (irrigation and row are collinear; see Study Design).

221 To approximate the impact from time of collection (row) in the vineyard on gene expression, linear

222 models were first fit to remove variation imparted by irrigation from each of the top 100 PCs. The

223 residuals were then used as the basis for linear models and machine learning analysis.

224

225 *Leaf Shape*

226   All leaves from a single shoot directly emerging from a trained cordon were collected from each

227 vine in the 288-vine set at anthesis and veraison. At harvest, we collected only the oldest (first emerging

228 leaf), middle (estimated from the middle of a whole shoot), and youngest (smallest fully emerged leaf at

229 the shoot tip, >1cm). Leaves were collected approximately in row order (from south to north) and stored

230 in a cooler. Each leaf was imaged using an Epson DS-50000 scanner in color against a white background

231 at 1200 DPI and written as JPEG formatted images. Following scanning of leaves for leaf shape analysis,

232 the oldest, middle, and youngest leaves were dried and used to estimate leaf elemental composition (see

233 Ionomics). As the leaf shape samples and ionomics samples were identical, 'block' represented

234 unmeasured spatial variation, but did not strictly correlate with time of sampling (see Methods). While all

235 leaves were collected from a single shoot, only the oldest, middle, and youngest leaves were used in this

236 analysis.

237   We assessed leaf shape using Generalized Procrustes Analysis (GPA) of landmarks. For the three

238 leaves per vine used in leaf shape analysis, 17 homologous landmark features were identified [22]. The

239 GPA-rotated coordinate space was used for all subsequent statistical analysis including PCA in order to

240   summarize variation in leaf shape [46]. From the PCA, we extracted the top 20 PCs and fit linear models

241   and machine learning models to describe variation.

242

243   *Vine physiology*

244   Intracellular CO_2 concentration, stomatal conductance and leaf transpiration rate were measured

245   at midday (each measured simultaneously between 10am to 1pm) on one fully expanded sun-exposed leaf

246   for each of the vines in the 72-vine set. Physiology measurements were taken in row order ensuring that

247   'block' correlated with temporal variation over the sampling window. Measurements were taken using an

248   LI-6400XT Portable Photosynthesis system coupled with a pulse amplitude-modulated (PAM) leaf

249   chamber fluorometer (Li-Cor, Inc., Lincoln, NE, USA) with the following parameters: incident

250   photosynthetic photo flux density level of 1000 µmol m−2 s−1 generated by a red LED array and 10%

251   blue light to maximize stomatal opening, CO_2 mixer of 400 µmol/s, fixed flow of 300 µmol/s, and

252   ambient leaf and block temperature. Soil moisture was measured for each plant in the 72-vine set using a

253   fieldScout TDR 300 Moisture meter equipped with 20 cm rods (Spectrum Technologies, Inc. Aurora, IL,

254   USA). Midday stem water potential was measured using a pressure bomb/chamber (PMS Instrument Co.,

255   Albany, OR, USA) after enclosing the leaves in an aluminum foil bag for at least 15 minutes to

256   equilibrate the water potential of the xylem in the stem to that attached leaf (for a discussion on

257   equilibration time, see [47,48]).

258

259   **Analyses**

260

261   *Leaf ionome*

262   To characterize the leaf ionome over the growing season, we sampled the youngest, middle, and

263   oldest leaf from a single shoot from each of the vines within the 288-vine set at three phenological stages

264   and measured the concentrations of 20 ions in each leaf individually. Bivariate correlations showed that

265   ion concentrations are not independent of each other, but that the strength and direction of relationships

266   between ions vary with respect to phenological stage and leaf position (Supplemental Figure 3). As such,

267   we fit independent linear models to each ion. Leaf position, phenological stage, or the interaction of

268   phenological stage and leaf position explained the highest amount of variation for most ions (Figure 1A-

269   B). Many ions significant for the interaction showed a clear signal of leaf position at anthesis and

270   veraison, and either no explainable variation or muted variation at harvest. For example, calcium (Figure

271   1B) varied with leaf position (22.7% variation explained; $p < 1e-05$), phenology (24.0%; $p < 1e-05$), and

272   their interaction (7.4%, $p < 1e-05$). All possible pairwise combinations of leaf position were significantly

273   different at anthesis, and both the youngest and middle leaves were different from the oldest leaves at

274   veraison and harvest. In the case of potassium (Figure 1B), significant variation was explained by leaf

275   position (16.1%; $p < 1e-05$), phenology (19.6%; $p < 1e-05$), and their interaction (10.6%; $p < 1e-05$).

276   However, post-hoc comparisons of phenology-wise mean calcium concentrations showed that differences

277   were present only at anthesis and veraison.

278   Rootstock genotype showed remarkable influence on the composition of the leaf ionome. All ions

279   except aluminum, sodium, and zinc were significant for rootstock as a single fixed effect (Figure 1A).

280   Rootstock explained between 0.4% (rubidium; $p = 3.2e-05$) and 14.3% (nickel; $p < 1e-05$) of variation ion

281   concentrations (Figure 1A). For some ion concentrations (such as cobalt and nickel), significant variation

282   was explained by the interaction of rootstock and phenology; this pattern was observed mostly in ions that

283   responded weakly to the interaction of leaf position and phenology. These ions showed similar patterns to

284   the leaf position by phenology interaction where a clear signal was exhibited at anthesis and veraison then

285   was either absent or muted at harvest. For example, cobalt was most abundant in '1103P'-grafted vines at

286   anthesis (Figure 1C). At veraison, both '1103P'-grafted and 'SO4'-grafted had elevated concentrations

287   compared to Ungrafted and '3309'-grafted vines. However, by harvest, cobalt concentration variation was

288   muted and only 'SO4'-grafted vines showed evidence of elevated concentration. Similarly, nickel showed

289   significant variation partitioned into the rootstock by the phenology effect (Figure 1C). Both anthesis and

290 veraison show reduced nickel concentration in '1103P'-grafted vines and elevated concentrations in

291 'SO4'-grafted vines. However, at harvest, no comparisons are significant.

292   Machine learning on ion concentrations confirms that the leaf ionome contains a signature from

293 the rootstock genotype and the interactions of rootstock genotype with phenology and leaf position. A

294 random forest model trained to predict rootstock showed an overall accuracy of 75.2% (Figure 1D). Ions

295 important for this classification were nickel (Mean Decrease in Accuracy (MDA)=0.089), molybdenum

296 (MDA=0.058), and magnesium (MDA=0.054), corroborating the rootstock term's significance in the

297 linear models. Notably, when we trained a model to simultaneously predict rootstock and phenological

298 stage, rootstock prediction accuracy increased appreciably (Figure 1E). For example, the ability of the

299 model to detect ungrafted vines (the balanced accuracy of ungrafted predictions) improved from 81.7%

300 accuracy overall to 91.1% accuracy at anthesis and 85.9% at harvest. Generally, performance at veraison

301 matched the rootstock-only model performance. The ions most important for this joint

302 (rootstock/phenological stage) prediction were nickel (MDA=0.167), phosphorus (MDA=0.110), and

303 strontium (MDA=0.065). The rootstock by phenology model term was significant in the linear models for

304 these ions, but was not a largest descriptor of variation. The joint prediction of rootstock and leaf position

305 performed substantially better than chance ($p < 1e-05$), but accounting for leaf position did not improve

306 rootstock prediction as was the case in the joint prediction of rootstock and phenology (Figure 1F). Ions

307 important for this classification were sulfur (MDA = 0.051), rubidium (MDA = 0.051), and nickel (MDA

308 = 0.049).

309

310 *Leaf metabolomics*

311   We performed untargeted metabolomics on leaves from the 72-vine set at veraison and harvest,

312 quantifying the concentrations of 661 metabolites (Figure 2). The top 20 PCs accounted for a total of

313 67.3% of the total metabolomic variation, with the top three capturing 23.1%, 9.2%, and 6.2%,

314 respectively. Individual PCs after the top 20 explained less than 0.82% of the metabolome. Linear models

315 for each of the top 20 PCs found that the strongest drivers of variation in leaf metabolomics were

316   phenology and temporal blocking factor. For example, 90.6% of variation on PC1 was due to phenology

317   (p < 1e-05; Figure 2A). PC2 primarily reflected the interaction of phenology and temporal block (26.4%,

318   p < 1e-05) and temporal block as a main effect (18.9%, p < 1e-05). The patterns of variation attributable

319   to PC2 were similar in PCs 3-10 (Figure 2A).

320   PC17 was controlled by rootstock as a main effect (18.5%, p < 1e-03; Figure 2B). On PC17,

321   ungrafted vines were significantly different from vines grafted to '3309C' (p = 0.02) and 'SO4' (p < 1e-

322   05). Vines grafted to '1103P' were also significantly different from vines grafted to 'SO4' (p = 0.009).

323   Metabolites that loaded more than 1.96 sd from the mean loading on PC17 were extracted and

324   independently fit to additional linear models. We identified four metabolite features (M374T1 [rt = 1.33,

325   m/z = 374.1146], M117T1 [rt = 0.61, m/z = 117.0583], M175T1_1 [rt = 0.87, m/z = 175.1269], and

326   M333T1_3 [rt = 0.71; m/z = 333.1582]) which were influenced by rootstock as a main effect and the

327   metabolite (M112T1 [rt = 1.48, m/z = 112.0061]) which was influenced by the interaction of rootstock

328   genotype and phenological stage. At this time, the identification of these features remains unknown.

329   Linear discriminant analysis confirmed that many experimental factors likely influence the

330   metabolome. For example, when trained to maximize variation between classes of rootstocks, the model

331   identified a space that weakly separates '1103P'-grafted and 'SO4'-grafted vines from ungrafted and

332   '3309C'-grafted vines (LD1) and separates '3309C'-grafted vines from other classes (on LD2) (Figure

333   2C). Despite this, machine learning showed minimal predictability for any class other than phenology,

334   which was predictable with an accuracy of 100% for withheld samples. Rootstock genotype based on the

335   metabolome was not predictable with accuracy only marginally better than chance (34.6%).

336

337   *Gene Expression*

338   We performed 3'-RNAseq on the youngest fully-opened leaves of the 72-vine set at three time

339   points (Figure 3). On average, each sample contained 4.1 million 3'-reads and measured the expression of

340   17,852 genes. Overall, we identified variation in 23,460 genes that had a DESeq2-normalized count

341   greater than two in at least five samples. We computed the expression of two classes of housekeeping

342   genes, and showed that they are generally stable across samples over phenological time (Supplemental

343   Figure 2). We noted that some variation is expected for housekeeping genes; see, for example, [49].

344   Moreover, we showed that patterns of previously annotated circadian genes conform to expected results

345   over the sampling window. For example, predicted orthologs of *LHY* and *RVE1* are correlated and

346   decreasing over our sampling window, and a predicted *TOC1* ortholog is invariant. The results of these

347   analyses provide general confidence in the gene expression data presented here.

348   Using a traditional differential expression analysis framework based on established DGE software

349   (Deseq2), all genes returned as significantly differentially expressed by rootstock appeared to be false

350   positives, evidenced by a single extreme outlier altering group means. Hierarchical clustering of the 500

351   most variable genes after variance stabilizing transformation (VST) showed strong latent structure in the

352   transcriptome and that most variation in the transcriptome was explained by the phenological stage

353   (Figure 3A). The top 100 PCs on the VST-transformed gene counts accounted for nearly 92.3% of

354   variation in the transcriptome. Linear models on each of the top 100 PCs indicated that 82.4% and 61.4%

355   of the variation on PC1 and PC2 respectively were attributable to the phenological stage (Figure 3B-C).

356   Row was also a significant descriptor of variation as a single, fixed effect and in interactions with

357   rootstock and phenological stage. For example, row accounted for 36.0% and 43.3% of the variation on

358   PC4 and PC6, respectively. Interacting with the phenological stage, row accounted for >10% of variation

359   on 17 additional PCs.

360   Patterns of gene expression identified through LDA corresponded to phenological stage, vine

361   row, and rootstock. LDA separated phenological stages into three distinct, non-overlapping groups in the

362   space spanning LD1 and LD2 (Supplemental Figure 4). When trying to separate rows into distinct classes,

363   the model converged on a 'horseshoe' shape in the LD1- LD2 space (Figure 3D), suggesting either a

364   circadian topology to the transcriptome or continuous spatial variation over the vineyard [50]. LD1

365   maximized the variation between row 8 (sampled early in the day) and row 16 (sampled a few hours

366   later). LD2 maximized the separation of both rows 8 and 16 with row 12 (the row sampled in the middle

367   of the sampling window). A model trained to separate rootstock classes (Figure 3E) showed that LD1

368 separated the rootstock 1103P from other rootstock genotypes, and LD2 primarily separated the rootstock

369 '3309C' from ungrafted vines (Supplemental Figure 4).

370   Formal machine learning on gene expression PCs largely supported the linear models. A random

371 forest trained to predict phenological stage classified testing samples with 92.9% accuracy. Anthesis was

372 the most predictable class with a balanced accuracy of 100%; veraison and harvest displayed balanced

373 accuracies of 92.7% and 92.4%, respectively. The PCs most important in phenology prediction were PC1

374 (MDA = 0.16) and PC2 (MDA = 0.12). Gene expression PCs were unable to predict rootstock, with a

375 total prediction accuracy of 23.4%. While no features were especially important in the prediction

376 processes, PC44 showed the largest mean decrease in Gini impurity corroborating its signal in the linear

377 models.

378

379 *Leaf shape*

380   We collected leaves from the 288-vine set at three time points and landmarked a total of 2,422

381 leaves (Figure 4). Homologous leaf landmarks were used for Generalized Procrustes Analysis (GPA).

382 PCA on the GPA-rotated coordinates revealed ~97.2% of the total shape variation was captured by the

383 top 20 principal components with PC1, PC2, and PC3 explaining 24.1%, 19.0%, and 13.3% of the

384 variation respectively. Lower values on PC1 primarily capture leaves with shallow petiolar sinuses and

385 short midvein distance from the depth of the superior sinus to the top of the midvein, whereas higher

386 values on PC1 capture the opposite (Figure 4A). Similarly, lower values on PC2 capture deep petiolar

387 sinuses combined with very shallow superior sinuses, and vice versa for higher values. PC3 primarily

388 captures asymmetry (Figure 4A).

389   In total, 5.76% of variation on PC1 was explained by the experimental design. Of this, variation

390 in leaf shape was explained by phenology (2.63%; padj < 1e-05), then rootstock (0.95%; padj < 0.001),

391 leaf position (2.61%; padj = 0.03), and the interaction of phenology and leaf position (0.62%; padj =

392 0.009) (Supplemental Figure 5A). Post-hoc mean comparisons on PC1 showed that shapes of leaves from

393 ungrafted vines were significantly different from leaves of vines grafted to 1103P (p < 0.001), 3309C (p <

394   0.001) and SO4 (p < 0.001) (Supplemental Figure 5B). Moreover, PC1 captured subtle variation in the

395   leaf position by phenological stage interaction where middle leaves showed significant differences

396   between anthesis and veraison (p < 1e-03), and the oldest leaves showed significant differences when

397   comparing anthesis to veraison (p < 1e-05) and anthesis to harvest (p < 1e-03).

398   For PC2, 61.4% of variation could be assigned to an experimental factor. This included

399   significant variation from leaf position (46.9%, padj < 1e-05), phenology (1.4%; padj < 1e-05), and the

400   interaction of leaf position and phenology (12.05%; padj < 1e-05; Figure 4D). Specifically, younger

401   leaves tended to have shallower sinuses and exaggerated superior sinus depths (higher values on PC2),

402   whereas older leaves tended to develop deeper petiolar sinuses and more shallow superior sinuses (lower

403   values on PC2). The degree of this separation decreased across the season, and the shapes converged on

404   the mean leaf shape on PC2, consistent with the middle leaf at all three phenological stages. PC2

405   additionally reflected the interaction of leaf position and rootstock (0.22%; p = 0.04; Supplemental Figure

406   5B), but post-hoc comparisons did not find any significant pairwise comparisons.

407   Machine learning on the GPA-rotated coordinate space identified moderate division of

408   developmental and phenological classes. Random forest models could predict the leaf position with

409   73.1% accuracy, with the most important feature being the y-component of the leaf apex (MDA = 0.051).

410   A model trained to predict phenology performed at 64.3% with the most important features being the x-

411   components of the points corresponding to superior sinus depth (left sinus MDA = 0.030, right sinus

412   MDA = 0.019). A model trained to predict rootstock performed only marginally better than chance at

413   28.1% accuracy.

414

415   *Vine physiology*

416   We measured intracellular CO_2 concentration (C_i), stomatal conductance (g_s), leaf transpiration,

417   water potential (ψ), and soil moisture for the 72-vine set (Figure 5). Each physiological phenotype varied

418   significantly across phenology and the block by phenology interaction (Figure 5A). For example, at

419   harvest, we observed specific differences in leaf CO_2 concentration (A vs C: p=0.003; B vs C: p=0.002)

420   and leaf transpiration (A vs B: p < 1e-03; A vs C: p < 1e-05; B vs C: p < 1e-05). Leaf transpiration and

421   stomatal conductance varied significantly with the interaction of rootstock and phenology. A post-hoc

422   comparison of means showed that leaf transpiration and stomatal conductances were elevated in

423   'Chambourcin' vines grafted to '1103P' at veraison as compared to leaves of ungrafted vines (leaf

424   transpiration: p = 0.001; stomatal conductance: p = 0.002 Figure 5B-C).

425

426

427   *Phenomic covariation*

428   Four leaf phenotyping modalities consisted of 10 or more measured phenotypes and were

429   measured for all plants in the 72-vine set (leaf ionome, leaf metabolomics, gene expression, leaf shape).

430   Using these data, we explored the extent to which different phenotypes (within and between modalities)

431   covaried over phenology and rootstock genotype (Figure 6; Supplemental Figure 6; Supplemental Figure

432   7). Within each phenotyping modality, we summarized the primary dimensions of phenotypic variation

433   using PCA (see Methods), so as to not weigh any modality too heavily. From each PCA, we extracted the

434   top 10 PCs, which explained a total of 88.9% of variation in the ionomics PCA (iPCA), 55.9% of the

435   variation for the metabolomics PCA (mPCA), 74.8% of the variation in the gene expression PCA (gPCA)

436   and 87.9% of the variation in the leaf shape PCA (sPCA).

437   Pairwise correlations of each PC within each phenological stage showed diverse correlation

438   magnitudes and directions both within a phenotyping modality and between phenotyping modalities

439   (Figure 6A-C; Supplemental Figure 6). Generally, the strongest relationships were between PCs within

440   phenotyping modalities. For example, the strongest correlations identified were between gene expression

441   PCs gPC1 and gPC2 at anthesis (r = 0.85, CI = [0.81, 0.87]; Supplemental Figure 6A, and metabolomics

442   PCs mPC1 and mPC2 at harvest (r = -0.78, CI = [-0.82. -0.76]). Correlations between modalities

443   represented a diversity of responses across phenological stages. For example, the correlation between

444   gene expression gPC4 and shape sPC3 was similar across the phenological stages, but only the correlation

445   at veraison was significant (r = 0.41, CI = [0.34, 0.47]; Supplemental Figure 6B). Correlations such as

446   between metabolomics mPC3 and gene expression gPC6 were similar and significant at both veraison (r =

447   -0.44, CI = [-0.50, -0.37]; Supplemental Figure 6C) and harvest (r = -0.37, CI = [-0.45, -0.28];

448   Supplemental Figure 5C). While many correlations varied over the course of the season, some

449   relationships entirely shifted in direction. For example, the correlation between metabolomics mPC3 and

450   mPC6 shifted from a positive significant relationship (r = 0.58, CI = [0.52, 0.63]) at veraison to a negative

451   significant relationship at veraison (r = -0.66, CI = [-0.73, -0.59]) (Supplemental Figure 6D).

452   Pairwise comparisons of PCs within each rootstock genotype show a suite of latent phenotypes

453   with significant presence/absence variation in significant correlations. Where each phenological stage

454   showed modularity by phenotyping modality, variation over rootstock genotype shows a strong ionomics

455   module with latent combination of other modalities interspersed (Supplemental Figure 7). For example, in

456   ungrafted vines, metabolomics mPC1 was correlated with four PCs from the ionome (Supplemental

457   Figure 7A). Each of the other rootstock genotypes had dramatically different topologies with the ionome

458   tending to be more connected within the ionome and connected to other modalities only on the periphery

459   (Supplemental Figure 7B-D). Examples of presence/absence variation were shown in small modules of

460   two latent phenotypes that were present in only one rootstock genotype. For example, in the ungrafted

461   vines, the correlation between gene expression gPC4 and metabolomics mPC3 was significant (r = -0.58,

462   CI = [-0.65, -0.51]) and, in '1103P'-grafted vines, the correlation between metabolomics mPC3 and shape

463   sPC6 (r = 0.59, CI = [0.53, 0.70]) was significant.

464

465   **Discussion**

466

467   In this study, we used grafted grapevines as an experimental system for characterizing root system

468   impacts on multi-dimensional leaf phenotypes over the course of a growing season. We detected

469   ubiquitous but subtle effects of the root system on all assayed modalities, and demonstrated that rootstock

470   influences on leaf phenotypes can be specific to the vine's developmental stage. The strongest signals of

471   rootstock influences on leaves were observed in the ionomics dataset, phenotypes for which the root

472   system has a noted and well-understood role.

473

474   *Phenology explains significant variation in all leaf phenotypes*

475   The timing of sampling or phenological stage of the vines (anthesis, veraison, harvest) was the

476   strongest driver of phenomic variation for most leaf phenotypes. For example, all 20 ions varied with

477   phenology and most ions showed that phenology, or the interaction of phenology with leaf developmental

478   position, was the strongest source of variation (Figure 1). Nearly one third of all measured transcripts

479   responded to seasonal variation, and the strongest effects on the transcriptome were phenology and row, a

480   correlate for the time within a three-hour sampling window. The only phenotype for which phenology

481   was not the most explanatory factor is leaf shape. Consistent with previous studies [23], we confirm that

482   most of the leaf shape variation reflects development along a single shoot, but much of this variation is

483   explained via interaction with phenology. These data highlight the dynamic nature of biological processes

484   taking place within grapevines over the course of a season.

485   The seasonal component to grapevine phenomic variation is a subject of much research,

486   especially in the berry. In studies designed to quantify molecular underpinnings of terroir, seasonal

487   variation was identified as the strongest signal in the metabolome [51–54]. Several studies have

488   characterized transcriptomic variation over the course of the season. For example, in conjunction with

489   metabolomics, seasonal variation of berry development was used to identify transcriptomic and

490   metabolomic developmental markers in 'Corvina' [55]. Follow-up analysis showed that nearly 18% of

491   transcripts varied seasonally [56]. Grapevine leaf shape also varies tremendously over the growing season

492   [23] and is stable over multiple growing seasons; interestingly, grapevine leaves are patterned in the

493   previous year, and the climate of the season in which the leaves were patterned influence aspects of leaf

494   shape [57,58].

495

496   *Grafting and rootstock genotype exhibit a complex and subtle signal on leaf phenotypes*

497   Consistent with previous studies, we confirm that grafting, as well as rootstock genotype, has a

498   complex effect on phenomic variation in the scion (the grafted shoot system). Most notably, we show that

499   the rootstock to which a scion is grafted influences ion concentrations in leaves. Rootstock genotype is

500   predictable from ion concentrations in the leaves, and this signal is strengthened when phenological stage

501   is included in the model. For example, we previously showed that nickel concentration was elevated in

502   vines grafted to the rootstock 'SO4' [19]. At a similar point in the season, we observe the same pattern,

503   but by harvest, nickel was almost entirely excluded from the leaf. This suggests that the biological

504   implications of this differential uptake could be missed if not surveyed across the season. We also

505   confirm that rootstock genotype influences the metabolome of grafted grapevine, in some cases in a

506   season-specific manner. In the transcriptome, PCA was able to identify dimensions of variation that were

507   significantly described by rootstock and the interaction of rootstock and time of day, confirming prior

508   observations [19]. Patterns of gene expression were associated with rootstock in some analyses; for

509   example, supervised methodologies identified linear discriminants in the PC space that separated gene

510   expression patterns of some rootstock genotypes. However, gene-by-gene analysis found no genes

511   modulated by rootstock genotype, or even just from the act of grafting that were not driven entirely by a

512   single outlier. We suspect these results are due, at least in part, to the strength of the phenology effect

513   overpowering more subtle variation imparted by rootstock genotype. Finally, of the physiology

514   phenotypes we measured, leaf transpiration and stomatal conductance were higher in vines grafted to

515   '1103P' in the middle of the season. Through these analyses, we have identified subtle but ubiquitous

516   effects of rootstock genotype on shoot system phenotype across modalities, and have shown that the

517   impact of grafting on leaf phenomic variation varies from one phenotype to the next.

518   Understanding the rootstock genotype influence on shoot system phenotypes is a growing area of

519   research, especially in grapevine. For example, in 'Cabernet Sauvignon', grafting increased ion uptake

520   globally and some rootstock genotypes provide a clear signal in the scion [28]. The wild *Vitis* species

521   from which the rootstocks were derived from (*Vitis berlandieri, V. riparia,* and *V. rupestris*) differ in root

522 architecture, preferred soil substrate, and genetic background; however, the specific aspects of their

523 biology that contribute to differences in ion uptake are not known [27]. To our knowledge, there is not yet

524 a strong causal link between the micronutrient component of the ionome and factors of vine growth or

525 development that might influence traits like wine quality. However, it is noted that macronutrient

526 deficiencies can have negative effects on such traits [59,60] and can be mediated by rootstock [61]. This

527 suggests a strong understanding of the rootstock influence on the vine's ionome is warranted, and more

528 work needs to be done to establish these relationships. Similarly, the metabolome is a key driver of the

529 formation of the graft junction and some key metabolites could be responsible for graft incompatibility

530 [62]. Building on this work, targeted metabolomics showed two classes of metabolites, flavanols and

531 stilbenes, were differentially abundant at graft junctions and in the rootstocks of 'Cabernet Sauvignon'

532 vines one month after grafting [63]. However, flavanols were not differentially abundant in the scion, but

533 scion stilbene concentrations were apparently controlled by rootstock genotype. The effect of rootstock

534 genotype on the scion transcriptome is perhaps the most varied. For example, 'Cabernet Sauvignon' shoot

535 apical meristems show no effects by rootstock genotype [14], but berries of the same cultivar do, although

536 the effect is tempered by seasonal variation [15]. Variation in 'Chambourcin' leaf shape was also driven

537 by rootstock genotype, especially in conjunction with differences in irrigation [19]. Collectively, these

538 studies all suggest that rootstock genotype influences scion phenotypes, but those effects will vary by

539 phenotype, scion genotype, and perhaps other experimental conditions.

540   Data presented here confirm and expand upon previous observations of rootstock effects on scion

541 phenotypes. Notably, this study was carried out using a robust experimental design (288-vine set and 72-

542 vine set comprising replicates of three rootstocks grafted with a common scion and an ungrafted control)

543 in a vineyard that had been in the ground for eight years at the time of sampling. Our coordinated

544 collection of five multi-dimensional leaf phenotypes, and inclusion of three sampling points spanning the

545 growing season allowed us to investigate the comprehensive nature of rootstock influences on the scion.

546 Further, this thorough analysis demonstrates that rootstock effects on scion phenotypes shift in magnitude

547   over the course of the season, indicating that aspects of time are tremendously influential to the observed

548   results regardless of phenotype.

549   While the results of previous studies on grafted grapevine are worthy of comparison, the work

550   presented here has a few limitations that render comparisons with other studies challenging for a variety

551   of reasons. One novelty in our study is the exploration of a hybrid grapevine system, 'Chambourcin'.

552   'Chambourcin' has a complex pedigree, including contributions from *Vitis riparia* and *V. rupestris*,

553   species which are each parent to two of the rootstocks used in this study [64]. Many of the significant

554   effects we observed in this study were subtle, which could reflect the genomic similarity between shoot

555   and root systems. It might be expected that rootstocks derived from *V. riparia, V. rupestris* and other

556   North American species might prompt more pronounced responses in European scions that lack North

557   American *Vitis* in their pedigrees. Moreover, our results were derived from data collected in a single year

558   at a single location. The phenotypes we measured are known to be heavily influenced by the environment,

559   and we expect some inter-annual variation in rootstock influences on shoot system phenotypes. This study

560   focused on a single scion, and as a result we are unable to explore how rootstock effects on shoot system

561   phenotypes vary across scions. To our knowledge, this is among the largest populations to have been

562   surveyed for such phenotypes in a near-decade-old established vineyard. While many studies have been

563   conducted in green houses or recently planted vineyards, the juxtaposition of our results and those

564   previously established serve as a powerful foundation for the generation of hypotheses for future studies.

565

566   *Phenomic covariation warrants work toward latent phenotypes*

567   In the present study, we assess the extent of covariation among leaf phenotypes. For the primary

568   dimensions of variation in each modality, within-modality correlations were strongest when accounting

569   for phenological timing. Correlations also existed between modalities, suggesting room for the analysis of

570   latent phenomic structure or targeted integrative analyses for experimental questions. For example,

571   aspects of the metabolome were frequently correlated with the transcriptome and leaf shape when

572   accounting for both phenological stage and rootstock genotype. Interestingly, correlations within and

573 between modalities were highly dynamic over a growing season and across rootstock genotype. For

574 example, several correlations with leaf shape were present at veraison, but were not detected at anthesis

575 and harvest. Moreover, the topology of connections in the ionomic network was variable over the

576 rootstock genotype (Supplemental Figure 6). This variation in topology confirms that root system

577 genotype has a strong influence on shoot system elemental composition, and suggests that root system

578 genotype can alter correlative patterns in the ionome. We believe phenomic covariation warrants further

579 investigation, specifically, by further including additional phenotypes such as lncRNA expression [65,66],

580 epigenetics [67], and microbiomes [68,69] which could yield more mechanistic understandings of the

581 influence of root systems on shoot systems and how plants interact with their environments through their

582 root systems. These mechanistic understandings could be used to further understand and optimize

583 consumer-facing traits such as fruit quality and yield. To date, much of the work constituting phenomics

584 in grapevine has addressed how berries develop over the growing season, how cultivars differ from one

585 another, and how the concept of terroir influences wine [51,52,55,70–72]. Despite data integration

586 techniques becoming more popular, there are still many open questions as to what analytical methods are

587 most appropriate and how to most effectively utilize them (reviewed for grapevine in [73,74]; reviewed

588 broadly in [75,76]). Ongoing work attempts to integrate high-dimensional phenomic datasets generated

589 within a single organ system (e.g., leaves); and future studies will expand this to explore phenomic

590 covariation in and among organs, over time, and across space.

591

592 **Potential Implications**

593   Our work on the influence of root system genotype on shoot system phenotype has broad

594 implications for a holistic understanding of how plants detect and respond to changing environmental

595 conditions, and how this response is coordinated among different organ systems. Data presented here

596 demonstrate that root systems that are genetically distinct from the scion exert influence on the scion,

597 leading to statistically significant differences in scion phenotypes based on the identity of their root

598 systems. This observation suggests that the above-ground phenotype results, at least in part, from below-

599   ground activity of the root system. Further, these data highlight the value of coordinated collection of

600   different multi-dimensional phenotypes for comparative studies, and for describing whole-plant

601   phenotypic shifts over seasons and in response to horticultural manipulations.

602   Beyond its use as an experimental model that is ideal for studying root/shoot interaction, grafting

603   is an important horticultural technique that is used in over 70 major crops. In grapevines, grafting was

604   developed primarily to combat the below-ground pest phylloxera, and grapevine rootstocks were selected

605   initially based on their resistance to this pest. Results presented here indicate that beyond phylloxera

606   resistance, grafting to genetically distinct rootstocks is a potential source of variation for the scion.

607   Ongoing work explores how root system impacts on shoot system phenotypes vary across scion

608   genotypes, and how the rootstock × scion interaction changes over space. The long-term implications of

609   this study are the potential honing of viticulture for future climates including the optimization of

610   rootstock-scion combinations based in part on an understanding of how rootstock effects on scion

611   phenotypes change over the course of the season. This work is relevant for breeding efforts, and may play

612   a role in the optimization of quantitative phenotypes such as vigor, fruit quality, and yield that may be

613   enhanced by, constrained by, or partially predicted from phenotypic variation elsewhere in the plant.

614

615   **Methods**

616

617   *Study Design*

618   Data were collected in 2017 from a split-plot experimental rootstock trial established in 2009 at

619   the University of Missouri's Southwest Research Center near Mount Vernon, MO (37.074167 N;

620   93.879167 W; Supplemental Figure 1). The rootstock trial includes the interspecific hybrid cultivar

621   'Chambourcin' growing ungrafted (own-rooted) and grafted to three rootstocks: '1103P', '3309C', and

622   'SO4' (Supplemental Figure 1D). Clonal replicates of each of the four rootstock-scion combinations were

623   planted 72 times for a total of 288 vines planted in nine rows. Each row was treated with one of three

624   irrigation treatments: full evapotranspiration replacement, partial (50%) evapotranspiration replacement

625   (reduced deficit irrigation; RDI), or no evapotranspiration replacement (Supplemental Figure 1A).

626   However, rainfall in 2017 likely mitigated the applied irrigation treatment (see Supplemental Note 1).

627   Vine position in the vineyard corresponded to time of sampling for some phenotypes (metabolomics, gene

628   expression, and physiology), as samples were taken from one end of the vineyard to the other over the

629   course of two to three hours. Because vineyard microclimates and sampling time may be associated with

630   phenomic variation, we defined 'block' as a factor that captures this spatial and temporal variation

631   inherent in sampling for those phenotypes. In the other phenotypes (ionomics and leaf shape), neither row

632   nor block correlated with time, so 'block' was simply a spatial covariate. Unique rootstock-scion

633   combinations were planted in cells of four adjacent replicated vines (Supplemental Figure 1A-B), with

634   rows consisting of eight cells (32 vines/row). To our knowledge, a field-planted rootstock experimental

635   vineyard of this size and age is rare. For some phenotypes (ionomics and leaf shape), it was possible to

636   collect samples from all vines in the experimental vineyard (the 288-vine set; Supplemental Figure 1A-

637   B). For other phenotypes (metabolomics, gene expression, and physiology), time and/or expense

638   associated with the phenotyping process required that we reduce sampling to a nested set of 72 vines

639   representing the middle two vines in each four-vine cell in the front half of the vineyard (the 72-vine set;

640   Supplemental Figure 1B-C). All phenotypes were assayed at three phenological stages: anthesis (~80% of

641   open flowers; 22 May 2017); veraison (~50% of berries had transitioned from green to red; 30 July 2017);

642   and immediately prior to harvest (25 September 2017). At each phenological stage, effort was made to

643   sample on days with full to partial sun and minimal precipitation.

644   This design was used to assess the following questions: 1) What is the influence of root system

645   genotype on shoot system phenotype? 2) How do systems of plant phenotypes vary over the growing

646   season and does rootstock genotype influence this variation? And 3) how do phenotypes covary within

647   and between phenotyping modalities?

648

649   *Linear Models*

650   Linear models were fit to the 20 measured ion concentrations, the top 20 PCs of the leaf

651   metabolome, the top 100 PCs of the leaf transcriptome, the top 20 PCs of leaf morphospace, and each

652   measured physiological trait. Outliers were detected using the R function 'anomalize' (options:

653   alpha=0.03, max_anoms=0.1). Each model was fit with fixed effect factors representing phenological

654   stage (anthesis, veraison, or harvest), rootstock (Ungrafted, '1103P', '3309C', or 'SO4'), leaf position

655   (youngest, middle, or oldest; only used in leaf morphology and leaf ion concentration models), and all

656   pairwise interactions of those terms. Both irrigation and block were included as fixed, non-interacting

657   effects with the exceptions of physiology and metabolomics, for which we allowed the interaction of

658   'Block' as it correlates with the time of sampling, potentially capturing temporal variation. Row, an

659   additional correlate for time and spatial variation, was included in place of a temporal block for the gene

660   expression models after removal of the variation attributable to irrigation, a factor collinear with row. All

661   linear models were interpreted using a type-3 sum of squares computation using the R package 'car' [77].

662   Estimated p-values for each term in the models were corrected for multiple tests (within phenotype) using

663   FDR correction as implemented by the R package 'stats' [78]. Results from the models are reported as the

664   variation explained by a particular term in the model and the estimated p-value. When appropriate, post-

665   hoc mean comparisons were computed using the package 'emmeans' [79]. Where multiple linear models

666   were being simultaneously interpreted, we applied a Bonferonni correction to reduce the number of false

667   positives.

668

669   *Machine Learning to Identify Rootstock Effects*

670   For visualization of between-class variation, we fit linear discriminant analysis models (LDA) to

671   each modality (ionomics, metabolomics, gene expression, and leaf morphology) using the 'lda' function

672   of the R package 'MASS' [80]. Projections of all samples into the LD space were plotted using ggplot2

673   [81]. In addition, we employed machine learning to capture subtle experimental effects. We partitioned

674   data from each modality into 80% training partitions and 20% testing partitions. Models were fit to

675 predict the phenological stage from which a sample was taken, the rootstock to which the scion was

676 grafted, and the joint prediction of phenology and rootstock. We also tested the predictability of leaf

677 position for ionomics and leaf shape, and the interaction of rootstock and leaf position for ionomics. We

678 used the 'randomForest' [82] implementation of the random forest algorithm. Models were fit and tuned

679 using the R package 'caret' [83]. Each performance was assessed using accuracy, with performance on

680 each class being assessed using the balanced accuracy, the midpoint of class-wise sensitivity and

681 specificity. Where appropriate, models were compared to 'chance', or the occurrence frequency of each

682 class. Confusion matrices were visualized from the out-of-bag predictions using 'ggplot2'. Important

683 features were identified from the randomForest object based on a phenotype-specific mean decrease in

684 model accuracy (MDA).

685

686 *Phenomic trait covariation*

687   We extracted ionomics, metabolomics, gene expression, and leaf shape data for the youngest

688 available leaf from the 72-vine set. Each data modality was summarized along the primary dimensions of

689 variation using PCA. For each class, we extracted the top 10 PCs and fit Pearson's correlations across all

690 pairs of PCs at each phenological stage. P-values from computed correlations were corrected using the

691 FDR method from the package 'stats' [84]. Correlations and their strengths were visualized using the R

692 package 'igraph' [85]. Example correlations were reported after running 10,000 bootstrapped subsamples

693 of 90% of data for paired phenotypes. From the distribution of estimated correlation coefficients,

694 confidence intervals were computed from the 0.025 and 0.975 quantiles. A subset of example correlations

695 were plotted using the R package 'ggplot2'.

696 **Availability of Code:**

697 All code to replicate the findings of this paper including shell scripts for RNAseq analysis and Jupyter

698 Notebooks for data analysis in R can be found on the Vitis Underground GitHub:

699 Project name: mt_vernon_2017_leaf

700 Project home page: https://github.com/PGRP1546869/mt_vernon_2017_leaf

701   Operating system(s): Platform independent

702   Programming language: R and Shell

703   Other requirements: R requirements are listed in the Jupyter Notebooks. Shell requirements: trimmomatic

704   v0.36, bbmap (Feb. 11, 2019), STAR v2.7.1a, htseq-count v0.11.2.

705   License: GNU GPL 3.0

706   Any restrictions to use by non-academics: None

707

708   **Data Availability:**

709   Raw metabolomics data are available at MetaboLights, accession MTBLS2831. Gene expression data are

710   available in the Sequence Read Archive under BioProject PRJNA674915. All other data supporting this

711   manuscript including ionomics, partially processed metabolomics, leaf scans, leaf landmarks, physiology

712   and weather data are available from figshare [86-90]. Other data further supporting this work are openly

713   available in the *GigaScience* repository, GigaDB [91]

714   **Declarations**

715   **Abbreviations:**

716   LC-MS: Liquid Chromatography Mass Spectroscopy; MS: Mass Spectroscopy; PCA: Principal

717   Components Analysis; PC: Principal Component; DPI: Dots per Inch; GPA: Generalized Procrustes

718   Analysis; PAM: Pulse Amplitude Modulated; MDA: Mean Decrease in Accuracy; rt: Retention Time;

719   m/z: Mass to charge ratio; LDA: Linear Discriminant Analysis; LD: Linear Discriminant; DGE:

720   Differential Gene Expression; pajd: Adjusted p-value; iPCA: ionomics PCA; mPCA: metabolomics PCA;

721   gPCA, gene expression PCA; sPCA: shape (morphology) PCA; CI: Confidence Interval; lncRNA: long

722   non-coding RNA; RDI: Reduced Deficit Irrigation

723   **Competing Interests:**

724   The authors declare that they have no competing interests.

725   **Funding**:

Figure Legends:

744   Figure 1: The ionome shows strong signal from rootstock genotype, leaf position, and phenological stage

745   (**A**) Percent variation captured in linear models fit to each of 20 ions measured in the ionomics pipeline.

746   Presence of a cell indicates the model term (top) was significant (FDR; p.adj < 0.05) for that ion (left).

747   (**B**) Example ions shown to vary significantly by the interaction of leaf position (Y=Youngest,

748   M=Middle, O=Oldest) and phenological stage in parts per million. Boxes are bound by 25th and 75th

749   percentile with whiskers extending 1.5 IQR from the box. Significant changes are indicated by letters

750   above boxes, and are only meant for comparison within each phenological stage. Group means are

751   displayed with black squares. (**C**) Example ions shown to vary significantly by the interaction of

752   rootstock genotype and phenological stage in parts per million. Significant changes are indicated by

753   letters above boxes, and are only meant for comparison within each phenological stage. Boxes are bound

754   by 25th and 75th percentile with whiskers extending 1.5 IQR from the box. Group means are displayed

755   with black squares. (**D**) Standardized heatmap for out-of-bag (OOB) predictions by a random forest

756   trained to predict rootstock genotype, (**E**) the interaction between rootstock genotype by phenology, and

757   (**F**) the interaction between rootstock genotype and leaf position.

758

759   Figure 2: The metabolome is influenced by rootstock genotype, phenological stage, and time of sampling.

760   (**A**) Percent variation captured in linear models fit to each of the top 20 principal components of the

761   metabolome (661 measured metabolites). Presence of a cell indicates the model term (top) was significant

762   for that PC (left, percent variation explained by the PC in parentheses). (**B**) The distribution of projections

763   onto PC17, the strongest captured rootstock effect in the metabolome. Boxes are bound by the 25th and

764   75th percentiles with whiskers extending 1.5 IQR from the box. (**C**) Projections of all samples into the

765   first two dimensions of a linear discriminant space trained to maximize variation between rootstock

766   genotypes.

767

768   Figure 3: Gene expression primarily responds to time of season and circadian correlates

769   (**A**) Heatmap showing 500 genes with the highest variance following the filtering of lowly expressed

770   genes and gene-by-gene variance stabilizing transformations (VST) ordered by example model factors

771   (below). (**B**) Percent variation captured in linear models fit to the top 100 Principal Components of the

772   VST-transformed gene-expression space. Presence of a cell indicates the model term (top) was significant

773   for that PC (left, percent variation explained by the PC in parentheses). (**C**) Projections of all samples into

774   the first two principal component dimensions to show that the largest descriptors of variation are due to

775   phenology. (**D**) Projections of all samples into the first two dimensions of the linear discriminant space

776   trained to maximize variation between the rows of the vineyard, and (**E**) rootstock genotype.

777

778   Figure 4: Leaf shape variation is primarily determined by shoot position but changes over the season

779   **(A)** Representative shapes showing leaf variation (-3 sd, mean, +3 sd) captured in each of the top 4

780   principal components of the Generalized Procrustes Analysis-rotated leaf shapes. **(B)** Projections of all

781   leaves into the first two dimensions of principal component space colored by the strongest determinant of

782   variation in the top two PCs. **(C)** Projections of all leaves into the first two dimensions of a linear

783   discriminant space trained to maximize variation between phenological stages. **(D)** Variation in leaf shape

784   captured on PC2 shown by leaf position and phenological stage. Large points represent the mean of the

785   group when projected onto PC2. Bars surrounding the mean show one standard deviation. Variation in

786   each group is shown as a composite leaf trace scaled to a standard size and centered over the mean.

787

788   Figure 5: Vine physiology varies with rootstock and the rootstock by phenology interaction

789   **(A)** Percent variation explained by model terms (top) from linear models fit to each of four physiology

790   traits (left). **(B)** Variation in leaf transpiration rate for each rootstock genotype over the course of the

791   season. Boxes are bound by the 25th and 75th percentiles with whiskers extending 1.5 IQR from the box.

792   Significant changes are indicated by letters above boxes, and are only meant for comparison within each

793   phenological stage. Group means are displayed with black squares. **(C)** Variation in stomatal conductance

794   for each rootstock genotype over the course of the season. Boxes are bound by the 25th and 75th

795   percentiles with whiskers extending 1.5 IQR from the box. Group means are displayed with black

796   squares. Significant changes are indicated by letters above boxes, and are only meant for comparison

797   within each phenological stage.

798

799   Figure 6: Phenomic covariation varies over the course of the season

800   Correlation networks showing patterns of covariation within and between phenotyping modalities. Nodes

801   of the network are connected if they are significantly correlated (Pearson, FDR; p.adj < 0.05). Edge

802   thickness is proportional to the strength of correlation (multiplied by 16 for visibility). Edge color reflects

803   the direction of the correlation where blue edges indicate positive correlations and orange edges indicate

804   negative correlations. Modalities are indicated by a leading character and node color: ionomics (iPCs;

805   purple), metabolomics (mPCs; pink), gene expression (gPCs; yellow), leaf shape (sPCs; green). Network

806   topologies are shown for **(A)** anthesis, **(B)** veraison, and **(C)** harvest.

807

808   **Figure Supplement Legends:**

809   Supplemental Figure 1: Experimental Design

810   **(A)** Vineyard Map. The vineyard features a randomized block design where 'Chambourcin' is grown

811   ungrafted and grafted to three rootstock genotypes: '1103P', '3309C', and 'SO4'. Each row is treated

812   with one of three irrigation treatments: full replacement of ET, reduced-deficit, no replacement of ET.

813   Each cell of the vineyard contains four replicate grafts. **(B)** Phenotype sampling scheme across the four

814   replicates in a cell. For example, the top panel (purple) shows all four vines in the first cell of Row 8 in

815   Block D. From each vine in that cell, ionomics and leaf shape were sampled. In contrast, the lower panel

816   shows the first cell in Row 8 in Block A. Here, the first and fourth replicates were sampled for ionomics

817   and leaf shape while the second and third replicates were sampled for all phenotypes. All vines (288)

818   were sampled for ionomics and leaf shape. The middle two vines in the front half of the vineyard (72

819   ) were additionally sampled for metabolomics, gene expression, and physiology. **(C)** Phenotype sample

820   scheme within a vine (along a shoot). For each plant, young leaves were sampled for ionomics, leaf

821   shape, and gene expression. Middle leaves were sampled for ionomics, leaf shape, metabolomics, and

822   physiology. Older leaves were sampled for ionomics and leaf shape. Samples for ionomics and leaf shape

823   were taken from the same shoot. All other phenotypes were sampled from independent shoots. **(D)**

824   Rootstock relatedness. Each of the rootstocks in this trial shares a parent species with a different

825   rootstock. '1103P' is a cross between *Vitis rupestris* and *V. berlandieri*. '3309C' is a cross between *V.*

826   *rupestris* and *V. riparia*. 'SO4' is a cross between *V. riparia* and *V. berlandieri*. The parent that is shared

827   between each pair of rootstocks is highlighted. This figure is partially reproduced from [19] available

828   under a Creative Common license (CC BY 4.0).

829

830   Supplemental Figure 2: Quality and validity assessment of 3' RNAseq data. **(A)** A survey of recently

831   annotated circadian clock orthologs from the grapevine genome annotation [44]. Orthologs surveyed

832   included the morning-phased RVE1 and LHY, evening-phased LUX and ELF4, and the nigh-phased

833   TOC1 **(B)** A survey of genes with housekeeping domains related to IPR000626 (ubiquitin) and

834   IPR004000 (actin).

835

836   Supplemental Figure 3:   Patterns of ion covariation change over experimental treatments

837   Correlation networks showing patterns of ion covariation across phenological stages and shoot position.

838   Nodes of the network are connected if they are significantly correlated (Pearson, FDR; p.adj < 0.05).

839   Edge thickness is proportional to the strength of correlation (multiplied by 16 for visibility). Edge color

840   reflects the direction of the correlation where blue edges indicate positive correlations and orange edges

841   indicate negative correlations.

842

843   Supplemental Figure 4: Patterns of variation contributing to gene expression linear discriminants

844   (**A**) Projections of leaf gene expression samples into the first two dimensions of a linear discriminant

845   space trained to maximize variation between phenological stages, rows in the vineyard, and rootstock

846   genotype. For each LD, the PCs that loaded significantly (>1.96 sd from the mean loading) are listed in

847   order of loading magnitude. (**B**) Distribution of the top loading PCs onto LD1 and LD2 for each of the

848   trained models.

849

850   Supplemental Figure 5: Patterns of variation in leaf shape are subtle

851   (**A**) Percent variation captured in linear models fit to each of the top 20 principal components of leaf

852   morphology. Presence of a cell indicates the model term (top) was significant for that PC (left, percent

853   variation explained by the PC in parentheses). (**B**) Composite leaf traces for the main rootstock genotype

854   effect identified on PC1.

855

856 Supplemental Figure 6: Example correlations within and between phenotyping modalities over the course

857 of the season

858 (**A**) Example correlation showing a strong within-modality correlation between the ionomics gPC1 and

859 gPC2 at anthesis. Pearson correlations by phenological stage and CIs derived from 10000 random 90%

860 draws are shown for each panel. Generally speaking, CIs overlapping with 0 were not accepted as

861 significant. (**B**) Example correlation showing one of the stronger between-modality correlations between

862 the gene expression gPC4 and morphology (shape) sPC3 at veraison. (**C**) Example correlation of a

863 relationship that is present multiple times over the course of the season between metabolomics mPC3 and

864 gene expression gPC6 at both veraison and harvest. (**D**) Example correlation that is dynamic over the

865 course of the growing season between the ionomics mPC3 and mPC6.

866

867 Supplemental Figure 7: Phenomic covariation varies over rootstock genotype

868 Correlation networks showing patterns of covariation within and between phenotyping modalities. Nodes

869 of the network are connected if they are significantly correlated (Pearson, FDR; p.adj < 0.05). Edge

870 thickness is proportional to the strength of correlation (multiplied by 16 for visibility). Edge color reflects

871 the direction of the correlation where blue edges indicate positive correlations and orange edges indicate

872 negative correlations. Modalities are indicated by a leading character and node color: ionomics (iPCs;

873 purple), metabolomics (mPCs; pink), gene expression (gPCs; yellow), leaf shape (sPCs; green). Network

874 topologies are shown for (**A**) Ungrafted, (**B**) '1103P'-grafted vines, (**C**) '3309C'-grafted vines, and (**D**)

875 'SO4'-grafted vines.

876

877 **References:**

878 1. Gehan MA, Fahlgren N, Abbasi A, Berry JC, Callen ST, Chavez L, et al.. PlantCV v2: Image analysis
879 software for high-throughput plant phenotyping. *PeerJ*. 5:e40882017;

880 2. Ubbens JR, Stavness I. Deep Plant Phenomics: A Deep Learning Platform for Complex Plant
881 Phenotyping Tasks. *Front Plant Sci*. 8:11902017;

882   3. Ubbens J, Cieslak M, Prusinkiewicz P, Stavness I. Latent Space Phenotyping: Automatic Image-Based
883   Phenotyping for Treatment Studies.

884   4. Soulé M. PHENETICS OF NATURAL POPULATIONS I. PHENETIC RELATIONSHIPS OF
885   INSULAR POPULATIONS OF THE SIDE-BLOTCHED LIZARD. *Evolution*. 21:584–911967;

886   5. Houle D, Govindaraju DR, Omholt S. Phenomics: the next challenge. *Nat Rev Genet*. 11:855–662010;

887   6. Mudge K, Janick J, Scofield S, Goldschmidt EE. A History of Grafting. In: Janick J, editor.
888   *Horticultural Reviews*. Hoboken, NJ, USA: John Wiley & Sons, Inc.; p. 437–93.

889   7. Pouget R. Histoire de la lutte contre le phylloxéra de la vigne en France: 1868-1895. *Hist Sci Med*.
890   INRA; 1990;

891   8. Walker MA, Lund K, Agüero C, Riaz S, Fort K, Heinitz C, et al.. BREEDING GRAPE
892   ROOTSTOCKS FOR RESISTANCE TO PHYLLOXERA AND NEMATODES - IT'S NOT ALWAYS
893   EASY. Acta Horticulturae.

894   9. Warschefsky EJ, Klein LL, Frank MH, Chitwood DH, Londo JP, von Wettberg EJB, et al.. Rootstocks:
895   Diversity, Domestication, and Impacts on Shoot Phenotypes. *Trends Plant Sci*. Elsevier Current Trends;
896   21:418–372016;

897   10. Tramontini S, Vitali M, Centioni L, Schubert A, Lovisolo C. Rootstock control of scion response to
898   water stress in grapevine. Environmental and Experimental Botany.

899   11. Bavaresco L, Lovisolo C. Effect of grafting on grapevine chlorosis and hydraulic conductivity. *VITIS-*
900   *Journal of Grapevine Research*. Citeseer; 2015;

901   12. Ferlito F, Distefano G, Gentile A, Allegra M, Lakso AN, Nicolosi E. Scion–rootstock interactions
902   influence the growth and behaviour of the grapevine root system in a heavy clay soil. Australian Journal
903   of Grape and Wine Research.

904   13. Ordish G. The great wine blight. J.M. Dent & Sons;

905   14. Cookson SJ, Ollat N. Grafting with rootstocks induces extensive transcriptional re-programming in
906   the shoot apical meristem of grapevine. *BMC Plant Biol*. BioMed Central; 13:1–142013;

907   15. Corso M, Vannozzi A, Ziliotto F, Zouine M, Maza E, Nicolato T, et al.. Grapevine Rootstocks
908   Differentially Affect the Rate of Ripening and Modulate Auxin-Related Genes in Cabernet Sauvignon
909   Berries. *Front Plant Sci*. Frontiers; 2016; doi: 10.3389/fpls.2016.00069.

910   16. Berdeja M, Nicolas P, Kappel C, Dai ZW, Hilbert G, Peccoux A, et al.. Water limitation and rootstock
911   genotype interact to alter grape berry metabolism through transcriptome reprogramming. *Hortic Res*.
912   2:150122015;

913   17. Zombardo A, Crosatti C, Bagnaresi P, Bassolino L, Reshef N, Puccioni S, et al.. Transcriptomic and
914   biochemical investigations support the role of rootstock-scion interaction in grapevine berry quality. *BMC*
915   *Genomics*. 21:4682020;

916   18. Chitarra W, Perrone I, Avanzato CG, Minio A, Boccacci P, Santini D, et al.. Grapevine Grafting:
917   Scion Transcript Profiling and Defense-Related Metabolites Induced by Rootstocks. *Front Plant Sci*.
918   Frontiers; 2017; doi: 10.3389/fpls.2017.00654.

919   19. Migicovsky Z, Harris ZN, Klein LL, Li M, McDermaid A, Chitwood DH, et al.. Rootstock effects on
920   scion phenotypes in a "Chambourcin" experimental vineyard. *Hortic Res*. 6:642019;

921   20. Galet P. A Practical Ampelography: Grapevine Identification. Comstock Pub. Associates;

922   21. Mullins MG, Bouquet A, Williams LE. Biology of the Grapevine. Cambridge University Press;

923   22. Chitwood DH, Ranjan A, Martinez CC, Headland LR, Thiem T, Kumar R, et al.. A modern
924   ampelography: a genetic basis for leaf shape and venation patterning in grape. *Plant Physiol*. 164:259–
925   722014;

926   23. Chitwood DH, Klein LL, O'Hanlon R, Chacko S, Greg M, Kitchen C, et al.. Latent developmental
927   and evolutionary shapes embedded within the grapevine leaf. New Phytologist.

928   24. Klein LL, Caito M, Chapnick C, Kitchen C, O'Hanlon R, Chitwood DH, et al.. Digital Morphometrics
929   of Two North American Grapevines (Vitis: Vitaceae) Quantifies Leaf Variation between Species, within
930   Species, and among Individuals. *Front Plant Sci*. 8:3732017;

931   25. Grimes DW, Williams LE. Irrigation Effects on Plant Water Relations and Productivity of Thompson
932   Seedless Grapevines. *Crop Sci*. 30:2551990;

933   26. Williams LE, Grimes DW. Modelling vine growth-development of a data set for a water balance
934   subroutine. *Proceedings of the Sixth Australian Wine Industry Technical Conference*. p. 169–74.

935   27. Gautier A, Cookson SJ, Lagalle L, Ollat N, Marguerit E. Influence of the three main genetic
936   backgrounds of grapevine rootstocks on petiolar nutrient concentrations of the scion, with a focus on
937   phosphorus. *OENO One*. 54:1–132020;

938   28. Lecourt J, Lauvergeat V, Ollat N, Vivin P, Cookson SJ. Shoot and root ionome responses to nitrate
939   supply in grafted grapevines are rootstock genotype dependent: Rootstock and nitrogen supply affect
940   grapevine ionome. *Aust J Grape Wine Res*. 21:311–82015;

941   29. Salt DE, Baxter I, Lahner B. Ionomics and the study of the plant ionome. *Annu Rev Plant Biol*.
942   59:709–332008;

943   30. Baxter I. Ionomics: The functional genomics of elements. *Brief Funct Genomics*. 9:149–562010;

944   31. Ziegler G, Terauchi A, Becker A, Armstrong P, Hudson K, Baxter I. Ionomic Screening of Field-
945   Grown Soybean Identifies Mutants with Altered Seed Elemental Composition. The Plant Genome.

946   32. Oliver SG, Winson MK, Kell DB, Baganz F. Systematic functional analysis of the yeast genome.
947   *Trends Biotechnol*. 16:373–81998;

948   33. Tweeddale H, Notley-McRobb L, Ferenci T. Effect of slow growth on metabolism of Escherichia coli,
949   as revealed by global metabolite pool ("metabolome") analysis. *J Bacteriol*. 180:5109–161998;

950   34. Islam MN, Downey F, Ng CKY. Comparative analysis of bioactive phytochemicals from Scutellaria
951   baicalensis, Scutellaria lateriflora, Scutellaria racemosa, Scutellaria tomentosa and Scutellaria wrightii by
952   LC-DAD-MS. *Metabolomics*. Springer; 7:446–532011;

953   35. Tautenhahn R, Patti GJ, Rinehart D, Siuzdak G. XCMS Online: a web-based platform to process
954   untargeted metabolomic data. *Anal Chem*. 84:5035–92012;

955   36. Tandonnet S, Torres TT. Traditional versus 3' RNA-seq in a non-model species. *Genom Data*. 11:9–
956   162017;

957   37. Bolger AM, Lohse M, Usadel B. Trimmomatic: a flexible trimmer for Illumina sequence data.
958   *Bioinformatics*. 30:2114–202014;

959   38. Bushnell B. BBTools software package. *URL http://sourceforge net/projects/bbmap*. 2017;

960   39. Jaillon O, Aury J-M, Noel B, Policriti A, Clepet C, Casagrande A, et al.. The grapevine genome
961   sequence suggests ancestral hexaploidization in major angiosperm phyla. *Nature*. 449:463–72007;

962   40. Canaguier A, Grimplet J, Di Gaspero G, Scalabrin S, Duchêne E, Choisne N, et al.. A new version of
963   the grapevine reference genome assembly (12X.v2) and of its annotation (VCost.v3). *Genom Data*.
964   14:56–622017;

965   41. Dobin A, Davis CA, Schlesinger F, Drenkow J, Zaleski C, Jha S, et al.. STAR: ultrafast universal
966   RNA-seq aligner. *Bioinformatics*. 29:15–212013;

967   42. Anders S, Pyl PT, Huber W. HTSeq: Analysing high-throughput sequencing data with Python.

968   43. Love MI, Huber W, Anders S. Moderated estimation of fold change and dispersion for RNA-seq data
969   with DESeq2. *Genome Biol*. 15:5502014;

970   44. Carbonell-Bejerano P, Rodríguez V, Royo C, Hernáiz S, Moro-González LC, Torres-Viñals M, et al..
971   Circadian oscillatory transcriptional programs in grapevine ripening fruits. *BMC Plant Biol*. 14:782014;

972   45. Anders S, Huber W. Differential expression analysis for sequence count data. *Genome Biol*.
973   11:R1062010;

974   46. Dryden IL, Mardia KV. Statistical Shape Analysis: With Applications in R. John Wiley & Sons;

975   47. Shackel K, Gross R. Using midday stem water potential to assess irrigation needs of landscape valley
976   oaks. 2002;

977   48. Levin AD. Re-evaluating pressure chamber methods of water status determination in field-grown
978   grapevine (Vitis spp.). *Agric Water Manag*. Elsevier BV; 221:422–92019;

979   49. Liang W, Zou X, Carballar-Lejarazú R, Wu L, Sun W, Yuan X, et al.. Selection and evaluation of
980   reference genes for qRT-PCR analysis in Euscaphis konishii Hayata based on transcriptome data. *Plant
981   Methods*. Springer Science and Business Media LLC; 2018; doi: 10.1186/s13007-018-0311-x.

982   50. Podani J, Miklós I. Resemblance coefficients and the horseshoe effect in principal coordinates
983   analysis. *Ecology*. Wiley; 83:3331–432002;

984   51. Degu A, Hochberg U, Sikron N, Venturini L, Buson G, Ghan R, et al.. Metabolite and transcript
985   profiling of berry skin during fruit development elucidates differential regulation between Cabernet
986   Sauvignon and Shiraz cultivars at branching points in the polyphenol pathway. *BMC Plant Biol*.
987   14:1882014;

988   52. Anesi A, Stocchero M, Dal Santo S, Commisso M, Zenoni S, Ceoldo S, et al.. Towards a scientific
989   interpretation of the terroir concept: plasticity of the grape berry metabolome. *BMC Plant Biol*.
990   15:1912015;

991   53. Cuadros-Inostroza A, Ruíz-Lara S, González E, Eckardt A, Willmitzer L, Peña-Cortés H. GC-MS
992   metabolic profiling of Cabernet Sauvignon and Merlot cultivars during grapevine berry development and
993   network analysis reveals a stage- and cultivar-dependent connectivity of primary metabolites.
994   *Metabolomics*. 12:392016;

995   54. Dal Santo S, Fasoli M, Negri S, D'Incà E, Vicenzi N, Guzzo F, et al.. Plasticity of the Berry Ripening
996   Program in a White Grape Variety. *Front Plant Sci*. 7:9702016;

997   55. Zamboni A, Di Carli M, Guzzo F, Stocchero M, Zenoni S, Ferrarini A, et al.. Identification of putative
998   stage-specific grapevine berry biomarkers and omics data integration into networks. *Plant Physiol*.
999   154:1439–592010;

1000 56. Dal Santo S, Tornielli GB, Zenoni S, Fasoli M, Farina L, Anesi A, et al.. The plasticity of the
1001 grapevine berry transcriptome. *Genome Biol*. 14:r542013;

1002 57. Chitwood DH, Rundell SM, Li DY, Woodford QL, Yu TT, Lopez JR, et al.. Climate and
1003 Developmental Plasticity: Interannual Variability in Grapevine Leaf Morphology. *Plant Physiol*.
1004 170:1480–912016;

1005 58. Chitwood DH, Mullins J, Migicovsky Z, Frank M, VanBuren R, Londo JP. Vein-to-blade ratio is an
1006 allometric indicator of climate-induced changes in grapevine leaf size and shape. bioRxiv.

1007 59. Bravdo B. EFFECT OF MINERAL NUTRITION AND SALINITY ON GRAPE PRODUCTION
1008 AND WINE QUALITY. *Acta Horticulturae*. 512:23–302000;

1009 60. Brunetto G, Melo GWBDE, Toselli M, Quartieri M, Tagliavini M. The role of mineral nutrition on
1010 yields and fruit quality in grapevine, pear and apple. *Rev Bras Frutic*. FapUNIFESP (SciELO); 37:1089–
1011 1042015;

1012 61. Gautier A, Cookson SJ, Hevin C, Vivin P, Lauvergeat V, Mollier A. Phosphorus acquisition
1013 efficiency and phosphorus remobilization mediate genotype-specific differences in shoot phosphorus
1014 content in grapevine. *Tree Physiol*. Oxford University Press (OUP); 38:1742–512018;

1015 62. Canas S, Assunção M, Brazão J, Zanol G, Eiras-Dias JE. Phenolic compounds involved in grafting
1016 incompatibility of Vitis spp: development and validation of an analytical method for their quantification.
1017 *Phytochem Anal*. 26:1–72015;

1018 63. Prodhomme D, Valls Fonayet J, Hévin C, Franc C, Hilbert G, de Revel G, et al.. Metabolite profiling
1019 during graft union formation reveals the reprogramming of primary metabolism and the induction of
1020 stilbene synthesis at the graft interface in grapevine. *BMC Plant Biol*. 19:5992019;

1021 64. Migicovsky Z, Sawler J, Money D, Eibach R, Miller AJ, Luby JJ, et al.. Genomic ancestry estimation
1022 quantifies use of wild species in grape breeding. *BMC Genomics*. 17:4782016;

1023 65. Vitulo N, Forcato C, Carpinelli EC, Telatin A, Campagna D, D'Angelo M, et al.. A deep survey of
1024 alternative splicing in grape reveals changes in the splicing machinery related to tissue, stress condition
1025 and genotype. *BMC Plant Biol*. 14:992014;

1026 66. Harris ZN, Kovacs LG, Londo JP. RNA-seq-based genome annotation and identification of long-
1027 noncoding RNAs in the grapevine cultivar "Riesling." *BMC Genomics*. BioMed Central; 18:9372017;

1028 67. Williams BR, Edwards CE, Kwasniewski MT, Miller AJ. Epigenomic patterns reflect irrigation and
1029 grafting in the grapevine clone'Chambourcin'. *bioRxiv*. Cold Spring Harbor Laboratory; 2020;

1030   68. Marasco R, Rolli E, Fusi M, Michoud G, Daffonchio D. Grapevine rootstocks shape underground
1031   bacterial microbiome and networking but not potential functionality. *Microbiome*. 6:32018;

1032   69. Swift JF, Hall ME, Harris ZN, Kwasniewski MT, Miller AJ. Grapevine microbiota reflect diversity
1033   among compartments and complex interactions within and among root and shoot systems. bioRxiv.

1034   70. Palumbo MC, Zenoni S, Fasoli M, Massonnet M, Farina L, Castiglione F, et al.. Integrated network
1035   analysis identifies fight-club nodes as a class of hubs encompassing key putative switch genes that induce
1036   major transcriptome reprogramming during grapevine development. *Plant Cell*. Am Soc Plant Biol;
1037   26:4617–352014;

1038   71. Savoi S, Wong DCJ, Arapitsas P, Miculan M, Bucchetti B, Peterlunger E, et al.. Transcriptome and
1039   metabolite profiling reveals that prolonged drought modulates the phenylpropanoid and terpenoid
1040   pathway in white grapes (Vitis vinifera L.). *BMC Plant Biol*. 16:672016;

1041   72. Savoi S, Wong DCJ, Degu A, Herrera JC, Bucchetti B, Peterlunger E, et al.. Multi-Omics and
1042   Integrated Network Analyses Reveal New Insights into the Systems Relationships between Metabolites,
1043   Structural Genes, and Transcriptional Regulators in Developing Grape Berries (Vitis vinifera L.) Exposed
1044   to Water Deficit. *Front Plant Sci*. 8:11242017;

1045   73. Wong DCJ, Matus JT. Constructing Integrated Networks for Identifying New Secondary Metabolic
1046   Pathway Regulators in Grapevine: Recent Applications and Future Opportunities. *Front Plant Sci*.
1047   8:5052017;

1048   74. Fabres PJ, Collins C, Cavagnaro TR, Rodríguez López CM. A Concise Review on Multi-Omics Data
1049   Integration for Terroir Analysis in Vitis vinifera. *Front Plant Sci*. 8:10652017;

1050   75. Huang S, Chaudhary K, Garmire LX. More Is Better: Recent Progress in Multi-Omics Data
1051   Integration Methods. *Front Genet*. 8:842017;

1052   76. Stein-O'Brien GL, Arora R, Culhane AC, Favorov AV, Garmire LX, Greene CS, et al.. Enter the
1053   Matrix: Factorization Uncovers Knowledge from Omics. *Trends Genet*. 34:790–8052018;

1054   77. Fox J, Friendly M, Weisberg S. Hypothesis tests for multivariate linear models using the car package.
1055   *R J*. Citeseer; 5:39–522013;

1056   78. R Core Team. R: A language and environment for statistical computing. Vienna, Austria;

1057   79. Lenth R, Singmann H, Love J, Others. Emmeans: Estimated marginal means, aka least-squares
1058   means. *R package version*. 12018;

1059   80. Ripley BD. Modern applied statistics with S. Springer;

1060   81. Wickham H. ggplot2: Elegant Graphics for Data Analysis. Springer;

1061   82. Liaw A, Wiener M, Others. Classification and regression by randomForest. *R news*. 2:18–222002;

1062   83. Kuhn M. Predictive Modeling with R and the caret Package. *Google Scholar*. 2013;

1063   84. Team RC, Others. R foundation for statistical computing. *Vienna, Austria*. 32013;

1064   85. Csardi G, Nepusz T, Others. The igraph software package for complex network research.
1065   *InterJournal, complex systems*. 1695:1–92006;

1066   86. Harris, Zachary. 2017 Ionomics Data. figshare. 2020.
1067   https://doi.org/10.6084/m9.figshare.13200980.v1

1068   87. Harris, Zachary. 2017 Metabolomics Data. figshare. https://doi.org/10.6084/m9.figshare.13201043.v1

1069   88. Harris, Zachary. 2017 Leaf Shape Data. figshare. 2020.
1070   https://doi.org/10.6084/m9.figshare.13200953.v1

1071   89. Harris, Zachary. 2017_weather_data.csv. figshare. 2020.
1072   https://doi.org/10.6084/m9.figshare.13198682.v1

1073   90. Harris, Zachary. 2017 Physiology Data. figshare. 2020.
1074   https://doi.org/10.6084/m9.figshare.13201016.v1

1075   91. Harris ZN; Awale M; Bhakta N; Chitwood DH; Fennell A; Frawley E; Klein LL; Kovacs LG;
1076   Kwasniewski M; Londo JP; Ma Q; Migicovsky Z; Swift JF; Miller AJ: Supporting data for "Multi-
1077   dimensional leaf phenotypes reflect root system genotype in grafted grapevine over the growing season"
1078   GigaScience Database. 2021. http://dx.doi.org/10.5524/100956
1079
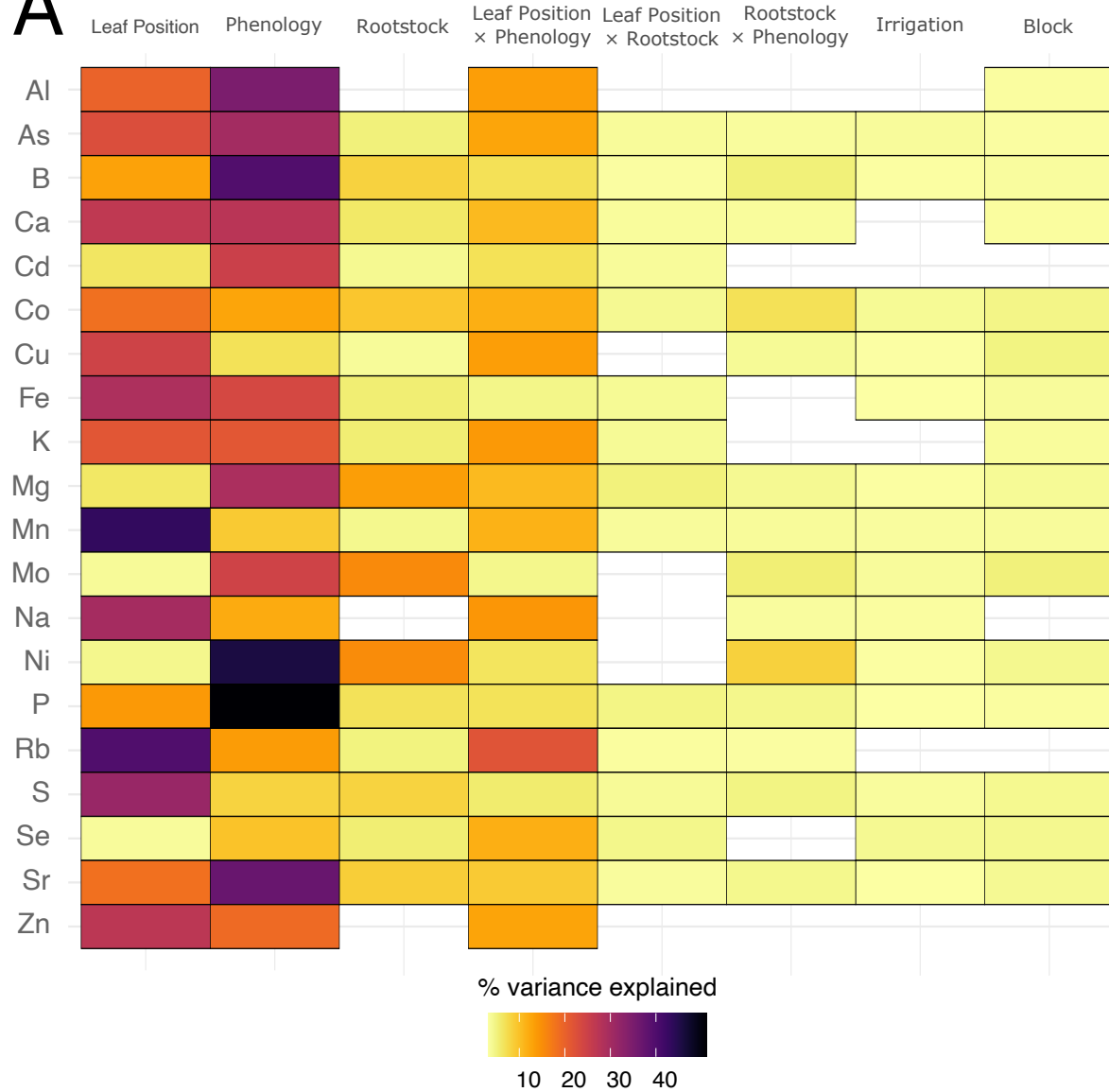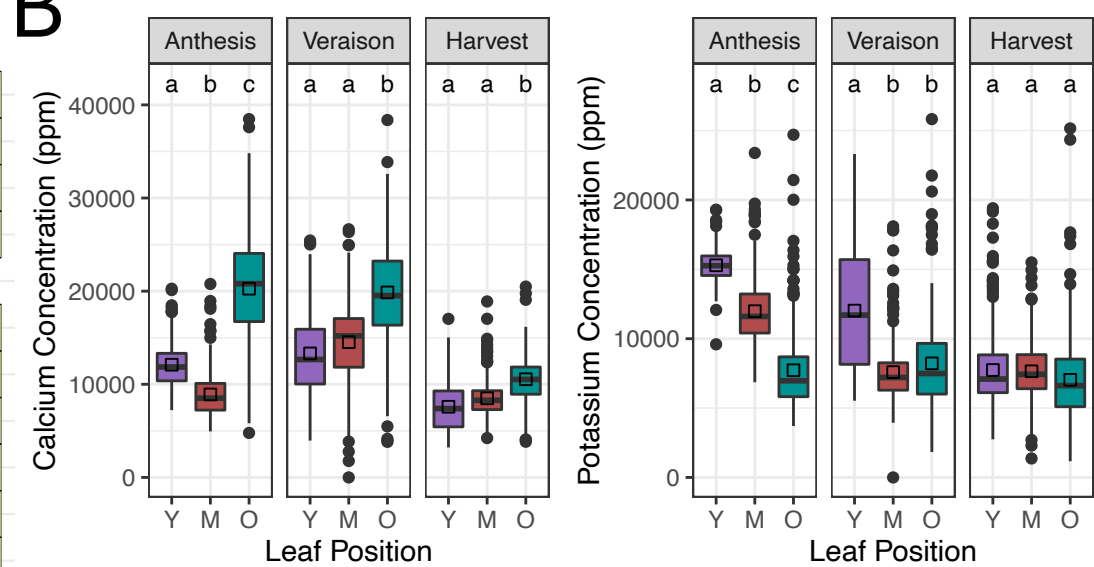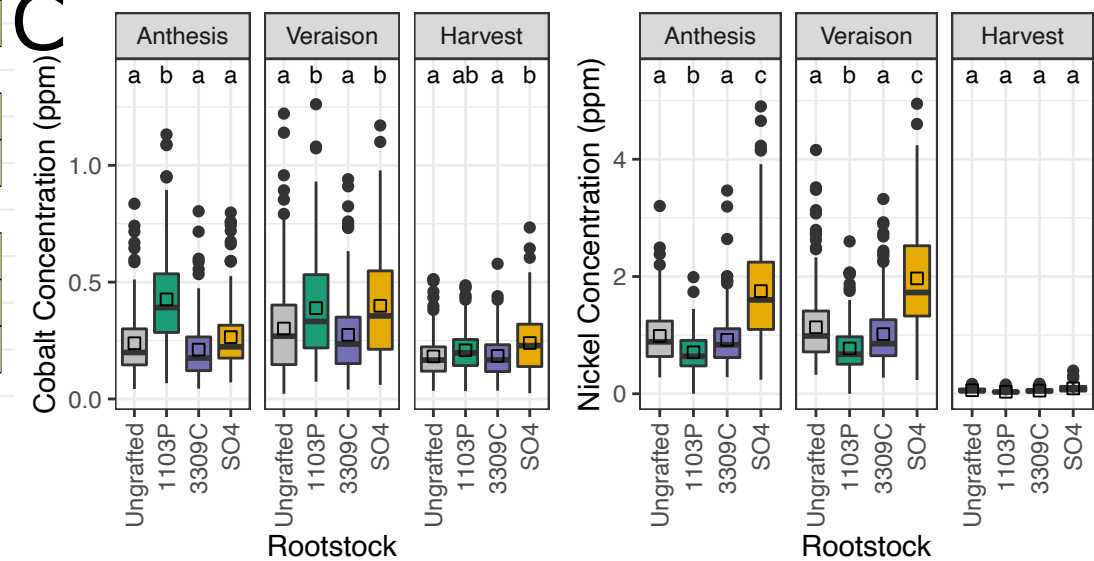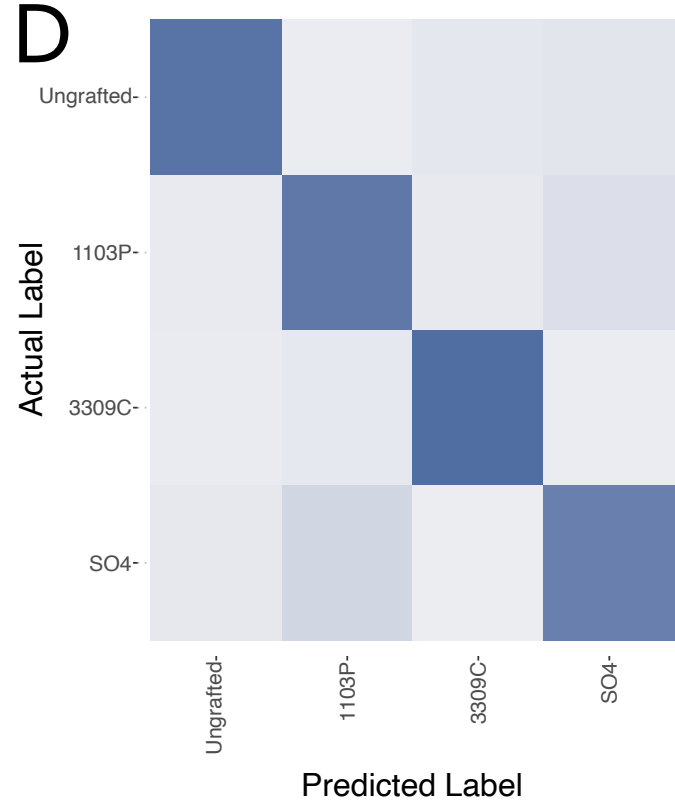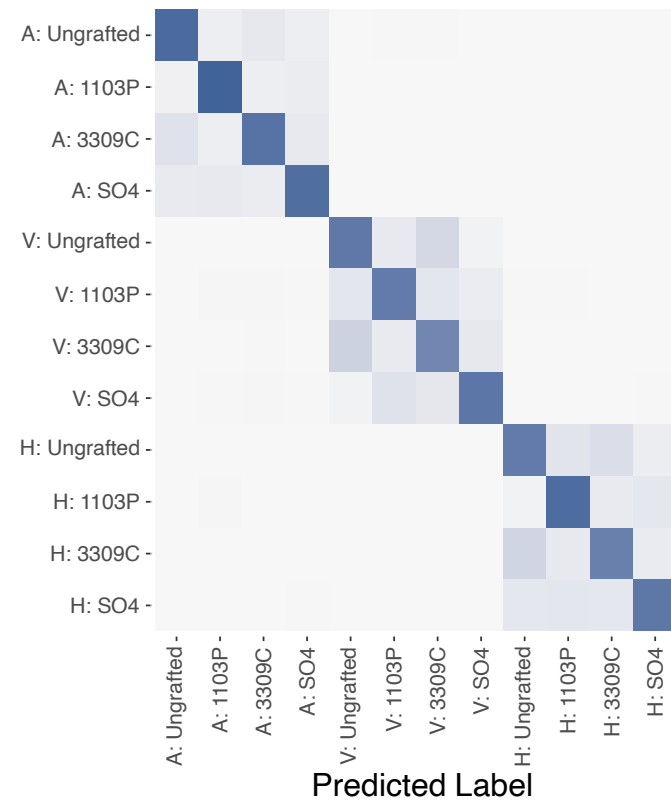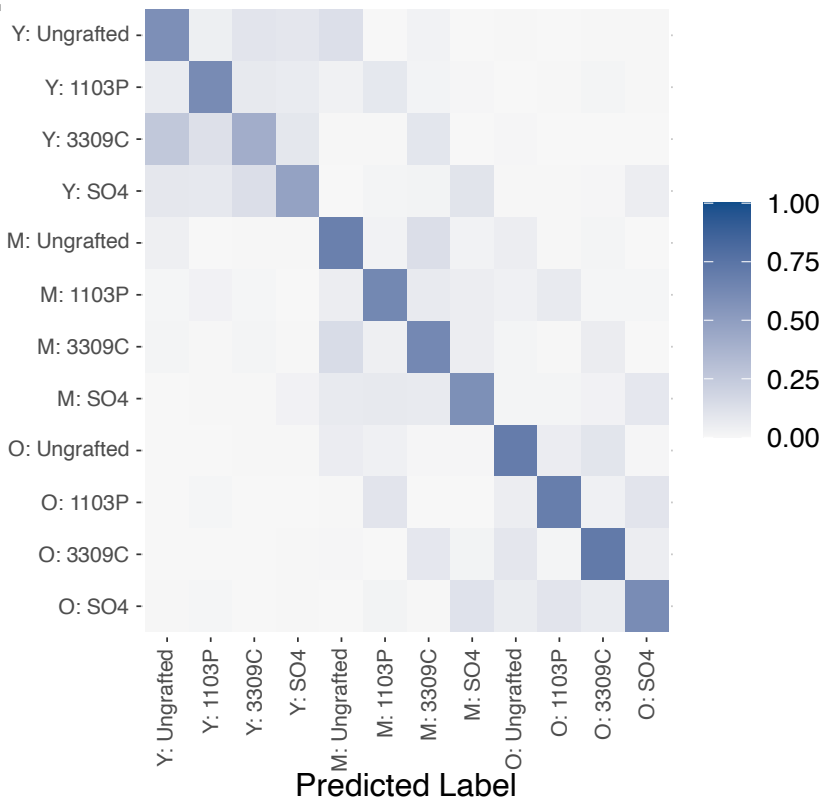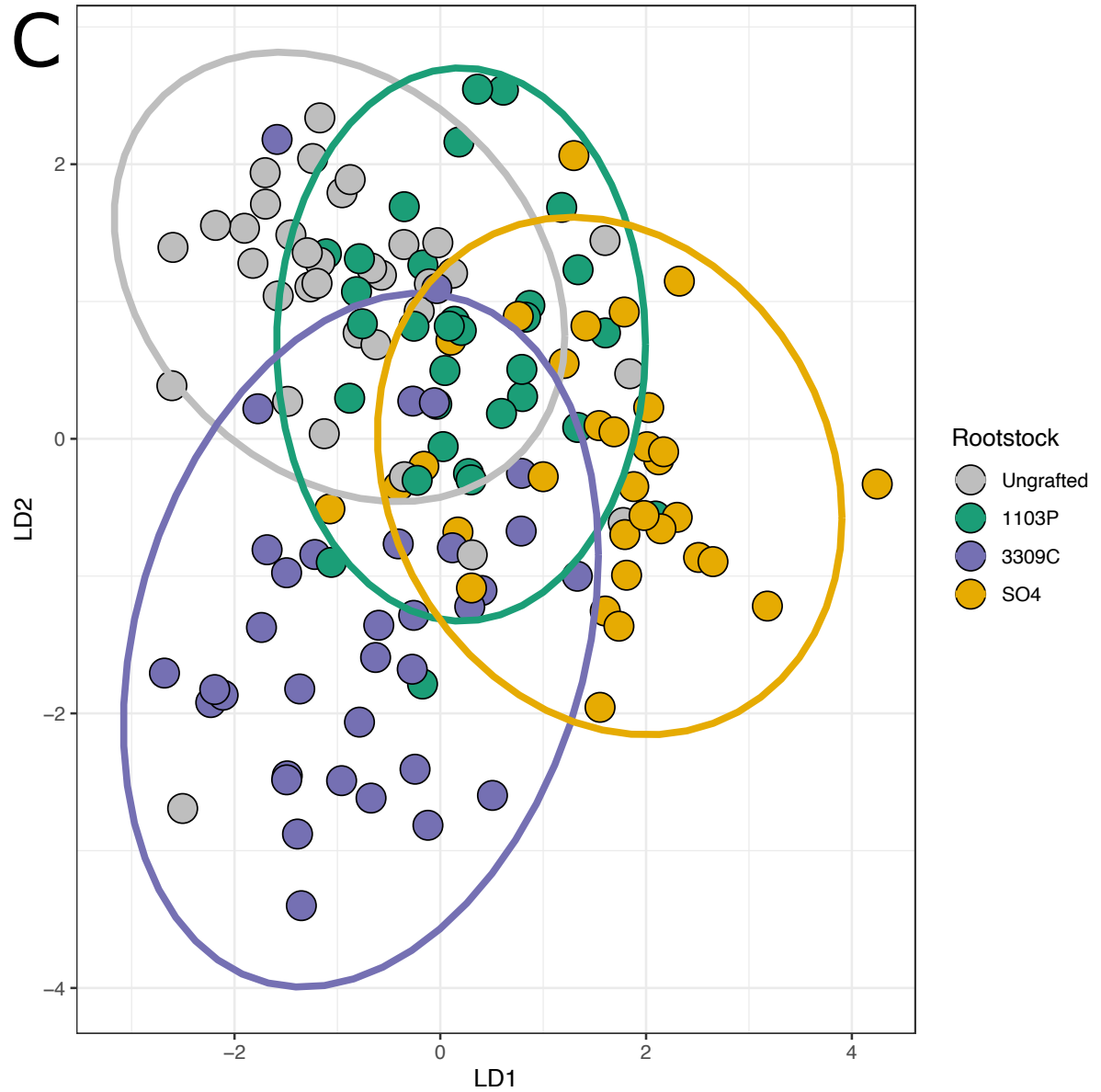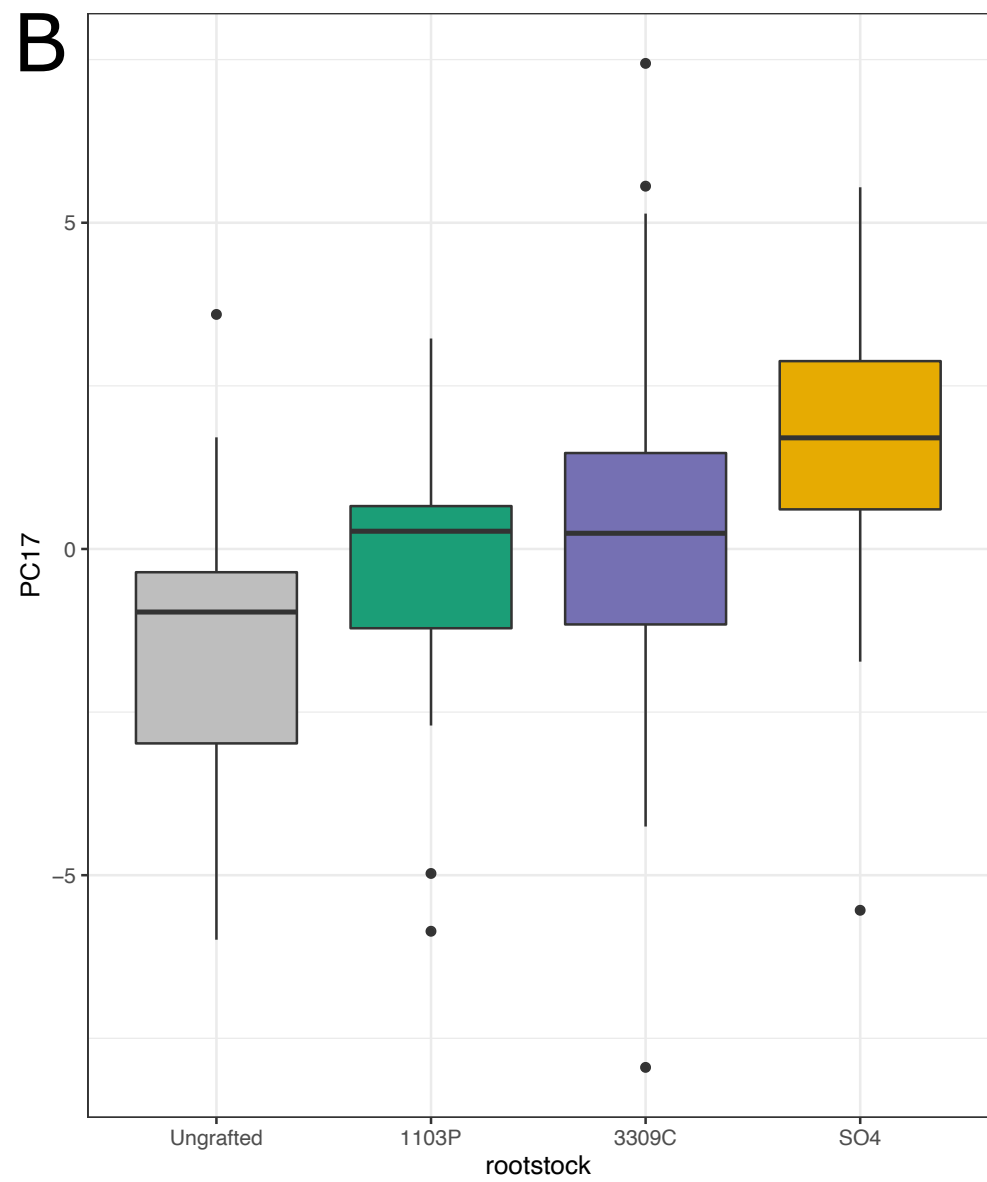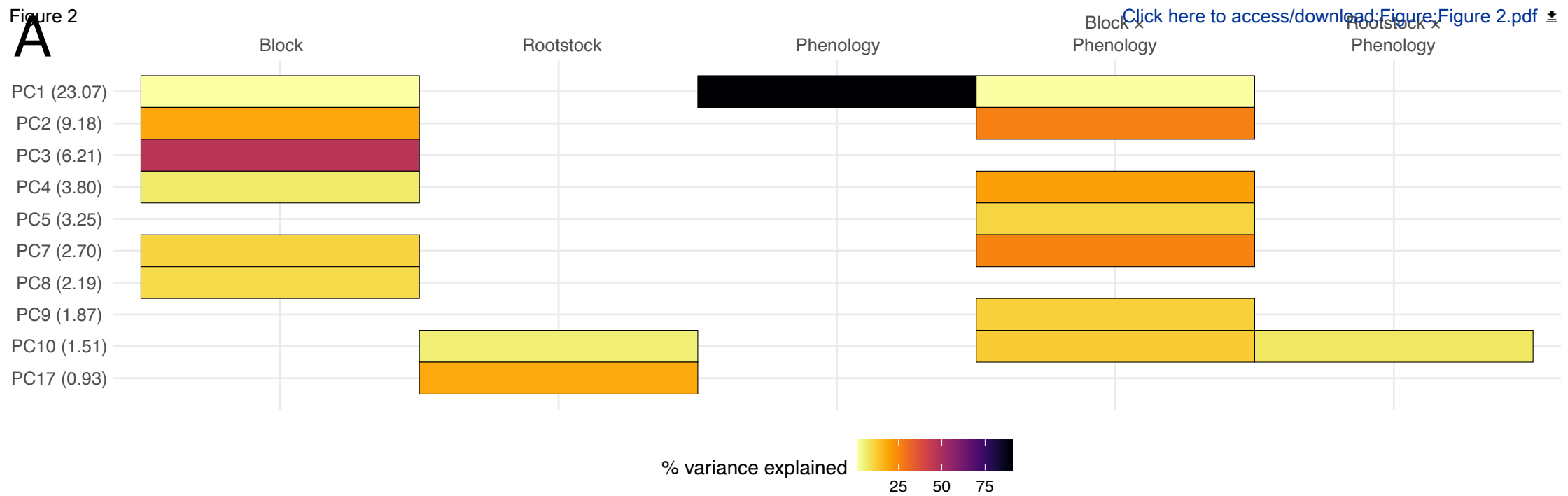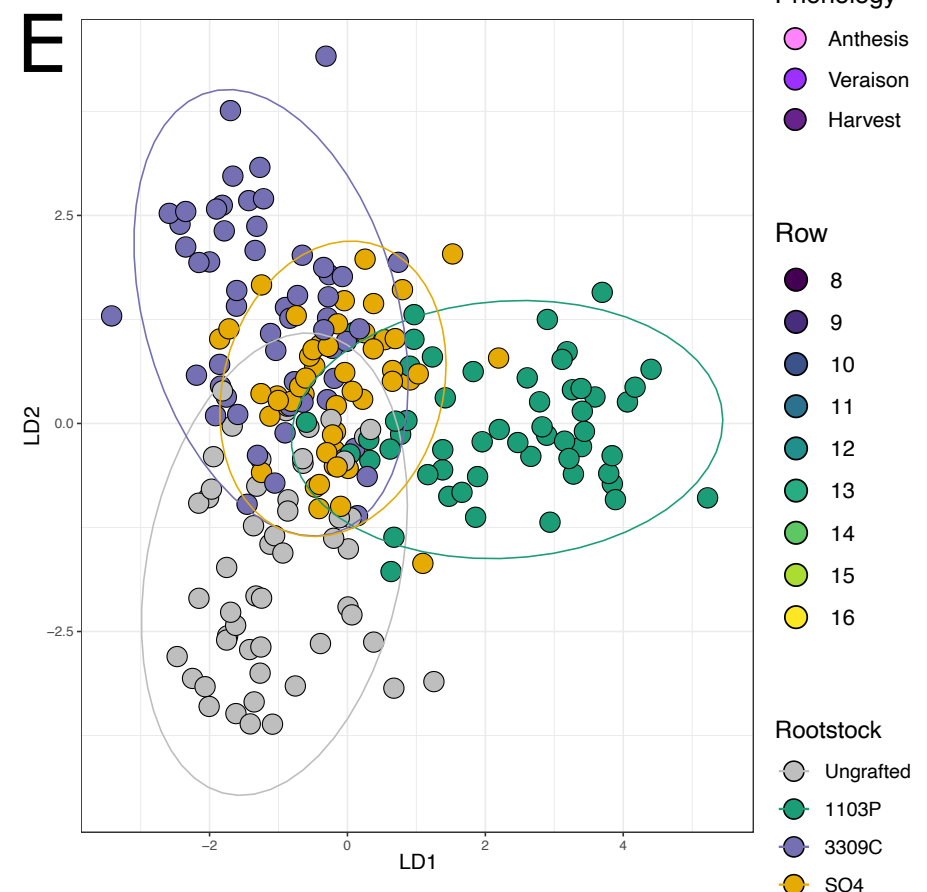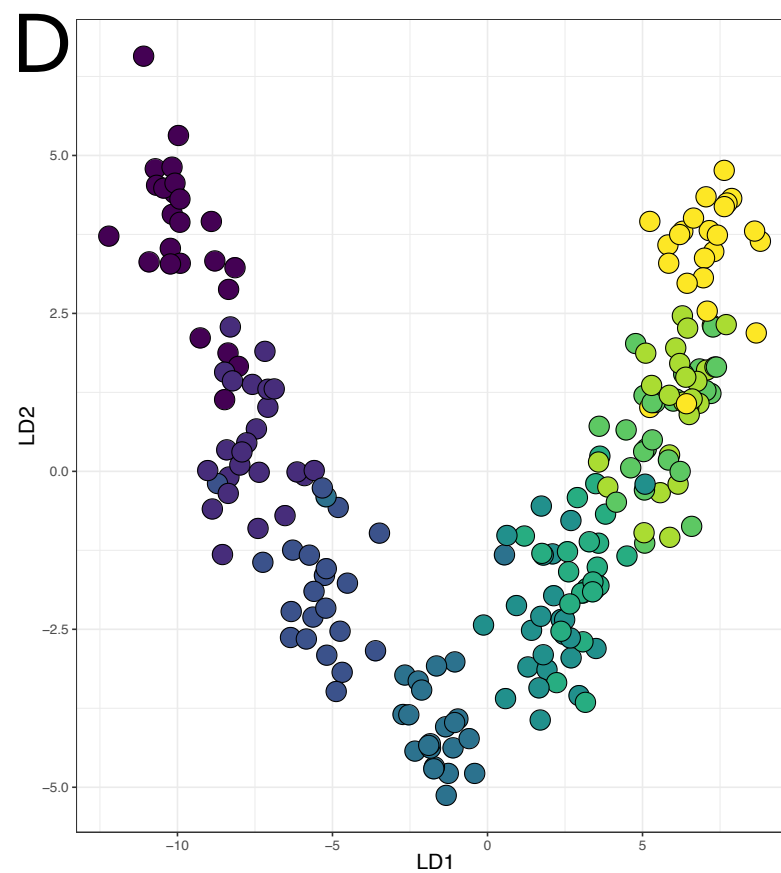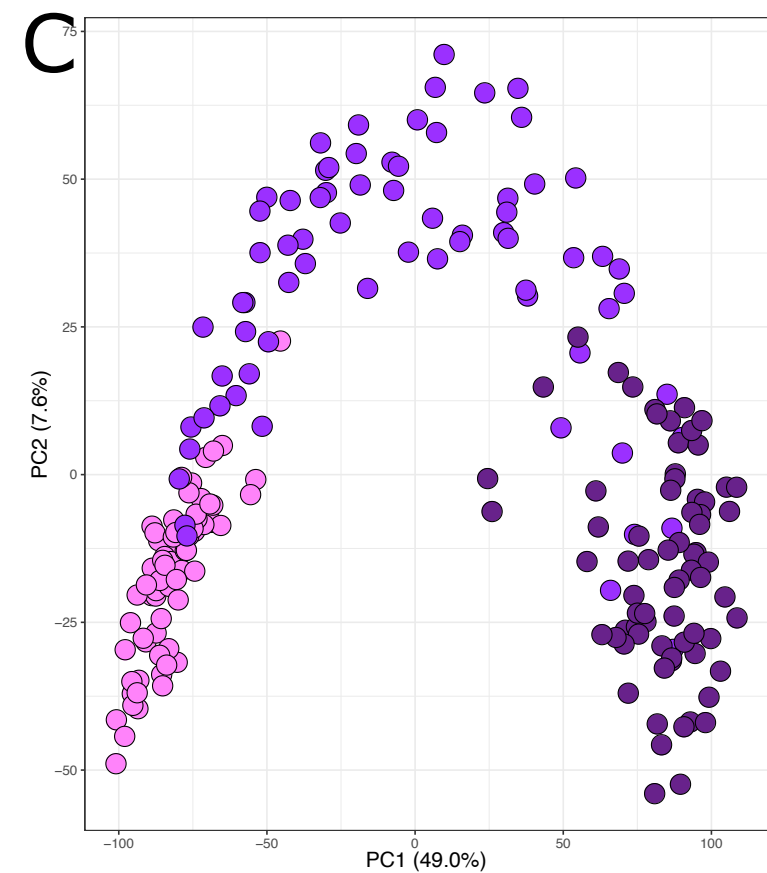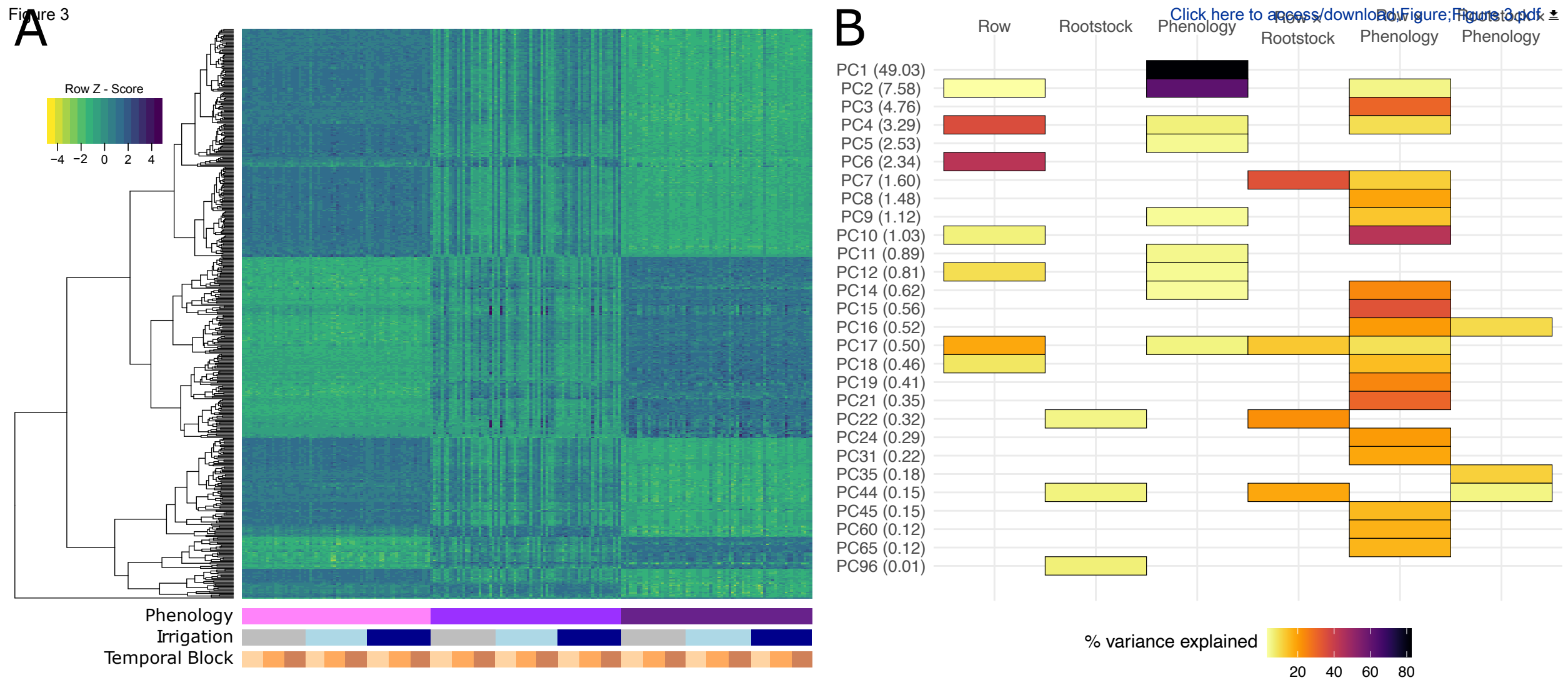
Figure 1

Figure 2

Figure 3

Figure 3
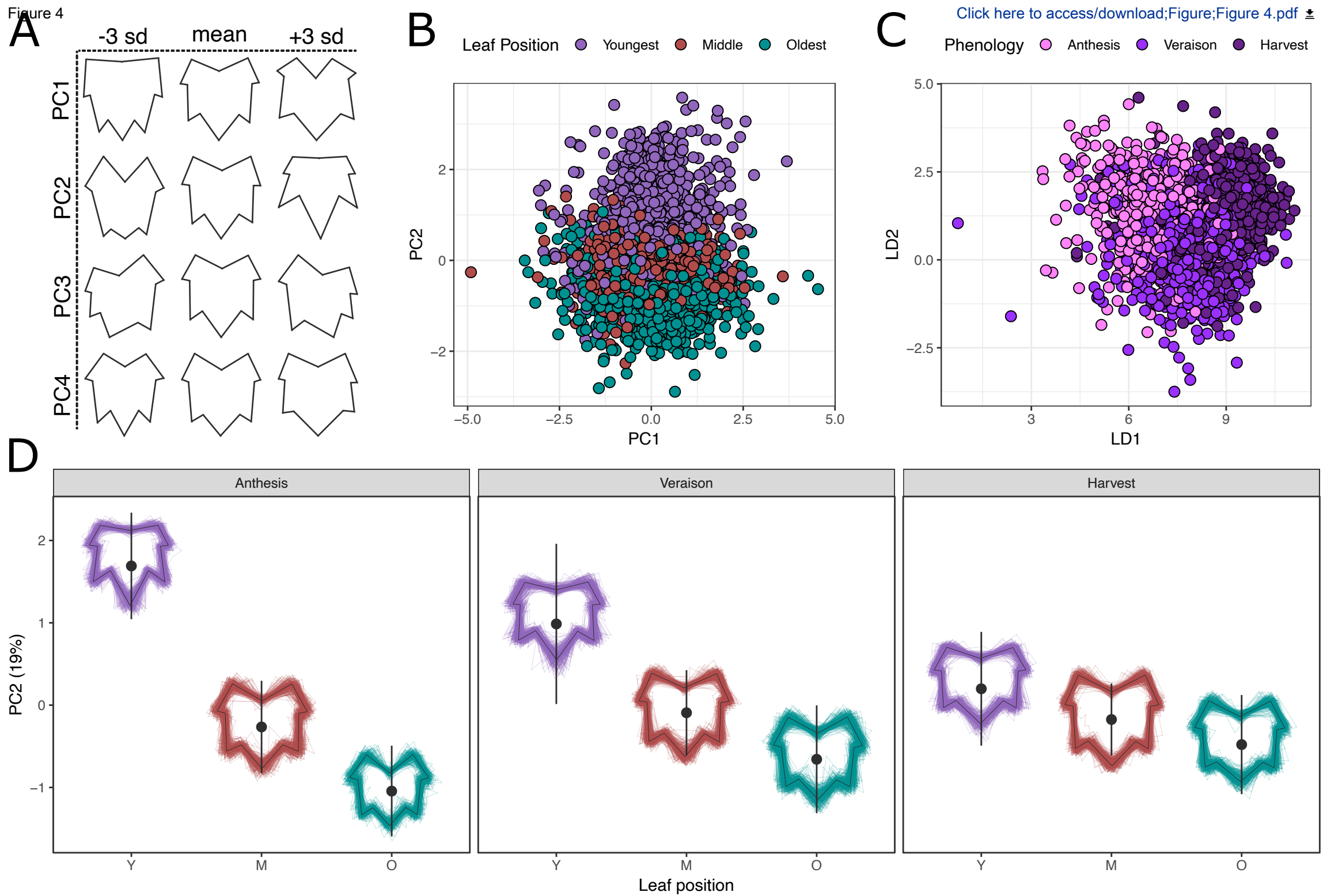
Figure 4

Figure 5

Figure 5

Figure 6

Ionomics (i)   Metabolomics (m)   Gene Expression (g)   Morphometrics (s)
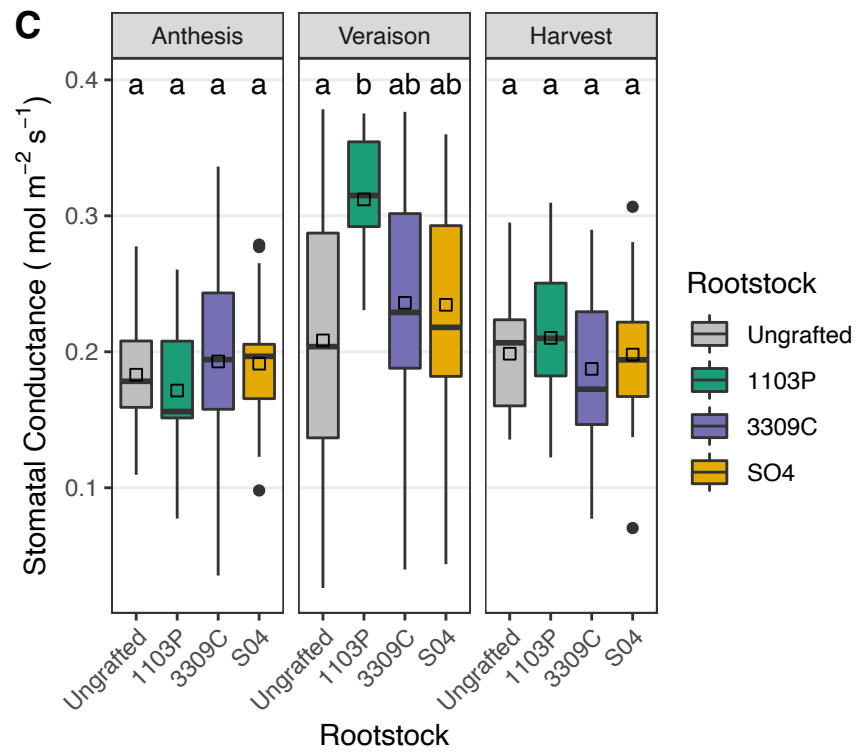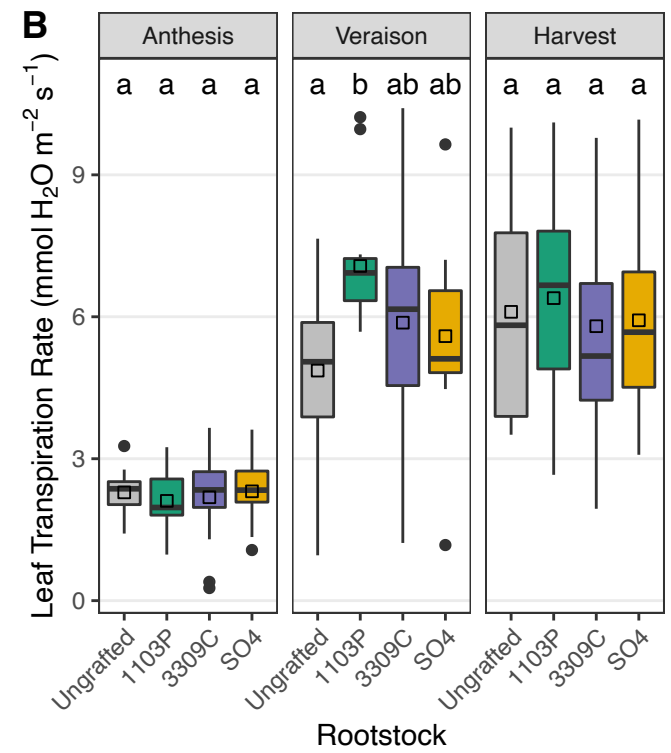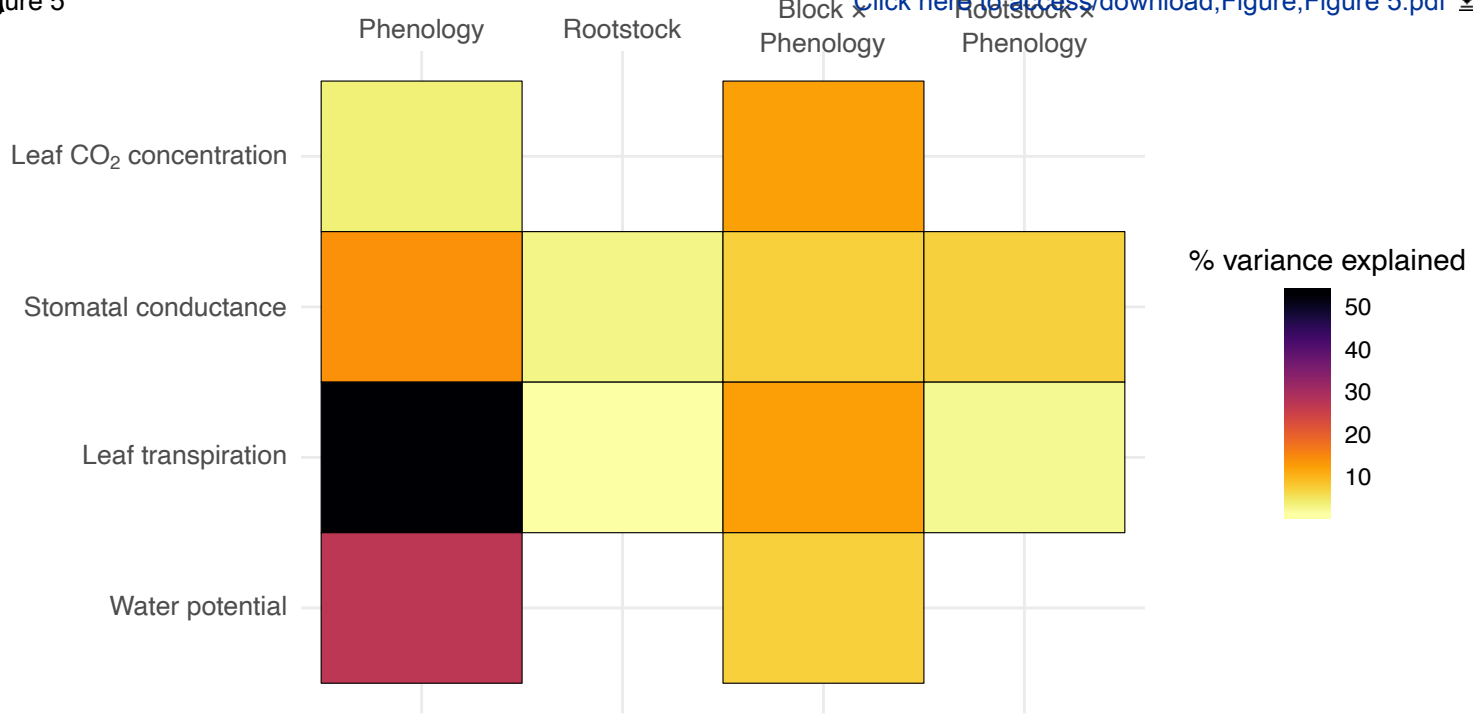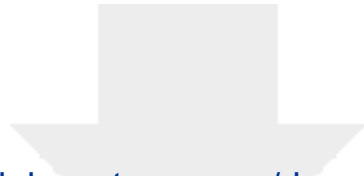
Supplemental Figure 1
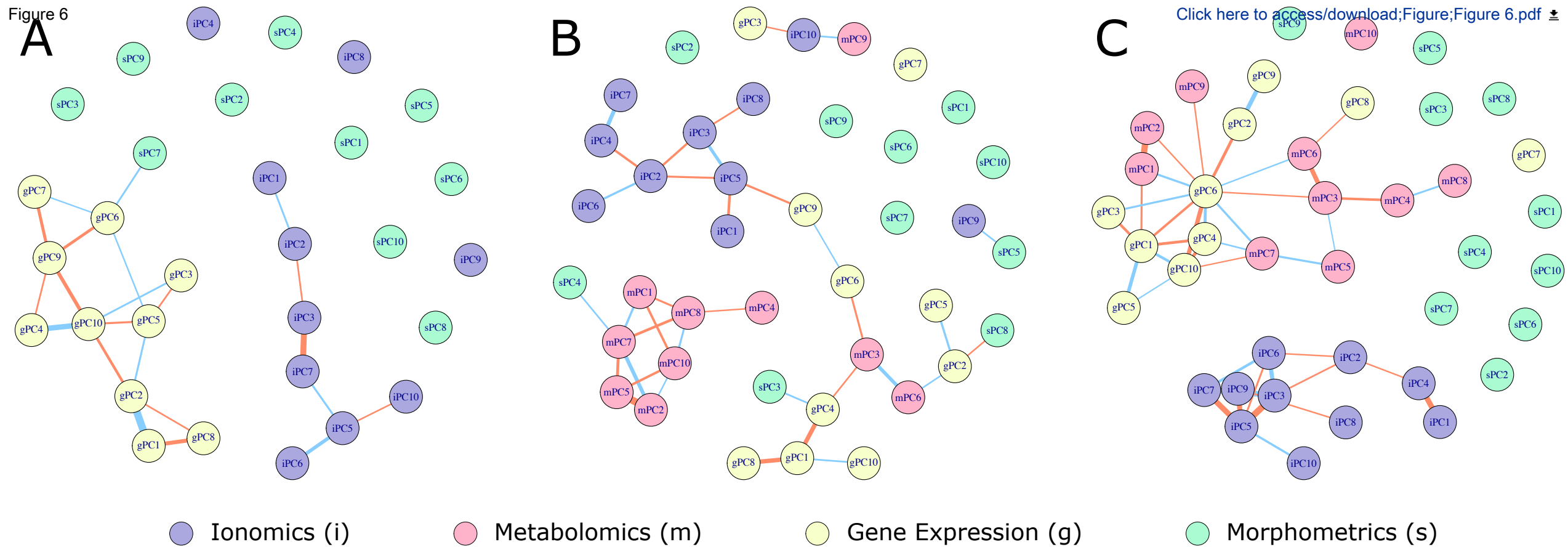
Click here to access/download
Supplementary Material
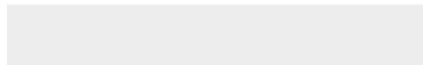Supplemental Figure 1.pdf
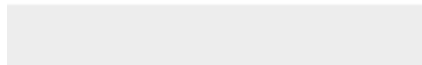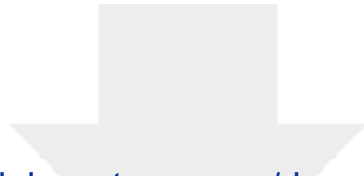
Click here to access/download
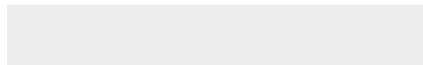**Supplementary Material**
Supplemental Figure 2.pdf

Click here to access/download
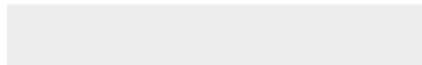**Supplementary Material**
Supplemental Figure 3.pdf

Click here to access/download
Supplementary Material
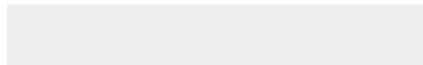Supplemental Figure 4.pdf

Click here to access/download
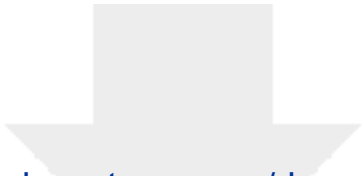**Supplementary Material**
Supplemental Figure 5.pdf

Click here to access/download
Supplementary Material
Supplemental Figure 6.pdf

Click here to access/download
Supplementary Material
Supplemental Figure 7.pdf

Click here to access/download
Supplementary Material
Supplemental Note 1.pdf

Dr. Nicole Nogoy,

We are happy to submit the revised version of our manuscript (GIGA-D-21-00137R2) with the suggested formatting revisions. To the best of our knowledge, we have addressed the requests of the editor and reviewers. If we missed anything by accident, please let us know and we will respond promptly to meet the journal and reviewer requirements. Thank you for your patience and support through this submission process, we are grateful for the guidance.

In this revision, we have addressed the following:
1. We have added information into the Code Availability Section so that it now meets the required format.
2. All figshare links were added to the references. Additionally, the GigaDB citation was added to the references. These are all referenced in the Availability of Data section. We also lightly edited the Availability of Data Section to be less redundant.
3. Abbreviations, Competing Interests, and Funding information has all been added/moved to the appropriate sections.

As the analysis scripts that we provided are very specific to the data at hand and are not a standalone software package, we have not sought registration with bio.tools or SciCrunch. If this is a misunderstanding on our part and needs to be completed, please let us know.

We look forward to hearing back.

Best,
Zachary N. Harris and Allison J Miller